A portable ECG data acquisition system using ADS1293

Srajan R
Dept. of Electronics and
Communication Engineering
N.M.A.M.Institute of Technology
Nitte, India
4nm20ec121@nmamit.in

Srinidhi Shet U
Dept. of Electronics and
Communication Engineering
N.M.A.M.Institute of Technology
Nitte, India
4nm20ec122@nmamit.in

Srinivas Prabhu
Dept. of Electronics and
Communication Engineering
N.M.A.M.Institute of Technology
Nitte, India
4nm20ec123@nmamit.in

Upendra Ashwin Pai
Dept. of Electronics and
Communication Engineering
N.M.A.M.Institute of Technology
Nitte, India
4nm20ec136@nmamit.in

Sukesh Rao M
Dept. of Electronics and
Communication Engineering
N.M.A.M.Institute of Technology
Nitte, India
sukesh@nitte.edu.in

*Abstract— **The ECG data acquisition module uses ADS1293 integrated chip (IC) to acquire bio potential and process the signals which should provide an easy and flexible user interface to the physician for examining the ECG over a standard chart on the portable display device. The proposed device should be capable of supporting the 3, 5, and 12 lead ECG systems. A single ADS1293 module has been used to demonstrate 3-Lead ECG data acquisition system. However, ADS1293 can also be used get 5 and 12 lead ECG system with addition modifications. The ADS1293 is driven using a 8 bit microcontroller unit (MCU) ATMEGA328 popularly known as Arduino UNO R3. The ADS1293 uses serial peripheral interface (SPI) communication protocol to connect with external MCU. The data captured from the ADS1293 is displayed on the serial plotter tool via universal asynchronous receive and transmit (UART) protocol.***

Keywords—Electrocardiogram, ADS1293, Arduino

I. INTRODUCTION

The Electrocardiogram (ECG), which is collected using electrodes positioned above the body, is a straightforward, safe, and graphical recording of the electrical activity of the heart and the variations that happen during cardiac contraction (systole) and relaxation (diastole) of the atria and ventricles during its operations.

Electric behavior was discovered earlier, in the 1790s, by Luigi Galvani (1737-1798). In 1791, he published his essay on "Effect of Electricity on Muscular Motion" [1]. His experiments on the frog were to determine the cause of muscle contractions. Galvani carried out numerous tests, but the most amazing one was when he put a frog's leg into a water-filled vessel and its nerve into another. He inserted a moistened paper between the vessels. The leg contracted as a result [2]. The Galvanometer was invented by this time. In 1828, Nobili added his galvanometer to Galvani's experiment plan. Carlo Matteucci (1811-1868) constructed his own galvanometer and obtained the same results as Galvani calling this current as "proper current" [2]. He was the first to observe the electric effect on a frog's heart when he placed Galvanoscopic frog against beating heart of another animal [3]. Augustus Desiré Waller (1856–1865) is recognized for developing the first real ECG. To capture the first "electrogram" from both animals and humans, he employed a Lippman capillary electrometer. He commented on his research in his speech in 1888, which also demonstrated that the contraction of the heart wasn't a simultaneous process but rather indicated start at the apex. and termination at the base [4]. Waller also noted the ventricular depolarization and repolarization. Willem Einthoven is credited for developing the electrocardiograph (1860–1927). In 1906, he devised another instrument-the string galvanometer. Einthoven was able to register good electrocardiographic representations and considered each cardiac contraction to have 5 deflections, labelled P, Q, R, S, and T [5].
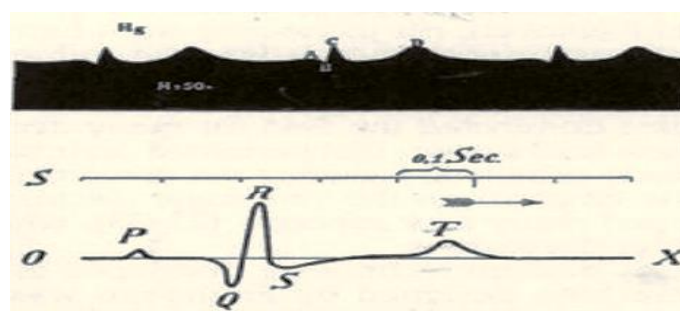

Fig.1 Electrocardiogram with P, Q, R, S, T zones [6]

II. ECG ELECTRODES AND LEADS

A. *ECG ELECTRODES*

An ECG electrode is a conductive pad that is attached to record electrical activity. The electrical activity of the heart is visualized graphically in an ECG lead, which is created by processing data from various ECG electrodes.

B. *3,5 AND 12 LEAD ECG*

3-lead ECG: To perform a 3-lead ECG, three electrodes must be positioned: one electrode next to each clavicle bone on the upper chest, and a third electrode close to the patient's lower left belly. The monitor reads Lead I, II, and III and it is a normal bipolar lead shape [7]. For rhythm monitoring, the Three-electrode ECGs simply record the limb leads [9]. A 3-lead ECG is the most common ECG for keeping track of a 24-hour readout. A 24-hour reading, which is compensated for as a long-term reading, is widely used to diagnose heart issues [8].

5-lead ECG: For a five-lead approach, the three electrodes in the three-lead configuration must be placed along with a fourth electrode next to the sternum (fourth intercostal gap on the right) and an additional electrode on the patient's lower right abdomen. The monitor reads Lead I, II, and III along with chest lead "C" because it is a bipolar lead form [7]. All six limb leads, and one chest view are recorded in a 5-electrode ECG [9].

12- lead ECG: Ten electrodes are required for a 12-lead configuration: the four electrodes that correspond to the patient's limbs are the left arm electrode (L lead), the right arm electrode (R lead), the left leg electrode (F lead), and the right leg electrode (N lead). Six chest electrodes (C1-C6 leads) are placed on the patient's chest in various places. To complete the 12 channel ECG, the recording consists of three augmented leads (aVR, aVL, and aVF), three bipolar leads (Lead I, II, and III), and six unipolar precordial leads [7]. A 12-lead ECG that provides information on both the vertical and horizontal axes is created by combining the lead systems from Einthoven, Goldberger, and Wilson. The 12-lead ECG, which is utilized for both resting and stress ECGs, is the gold standard for ECG diagnosis [8].
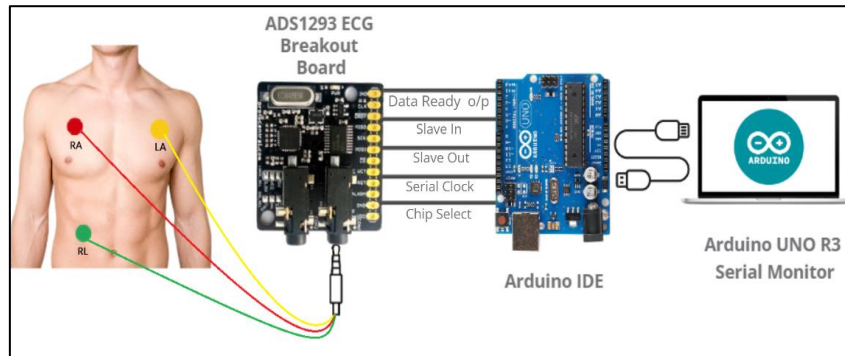
III. SYSTEM DESCRIPTION

Fig.2 Block diagram of the setup

A participant is attached with three leads namely RA - right arm, LA - left arm, and RL - right leg to acquire 3- Lead ECG. These leads are then connected to the ADS1293 ECG breakout board via a 3.5mm headphone jack. The SPI communication protocol is followed for the connection of the ADS1293 ECG breakout board with Arduino UNO as shown in TABLE I.

The Arduino sketch for the ECG breakout board is uploaded using Arduino IDE and the real-time ECG waveform is plotted using a serial monitor tool available on the Arduino IDE

TABLE I. SPI connection reference for ADS1293 ECG breakout board with Arduino UNO

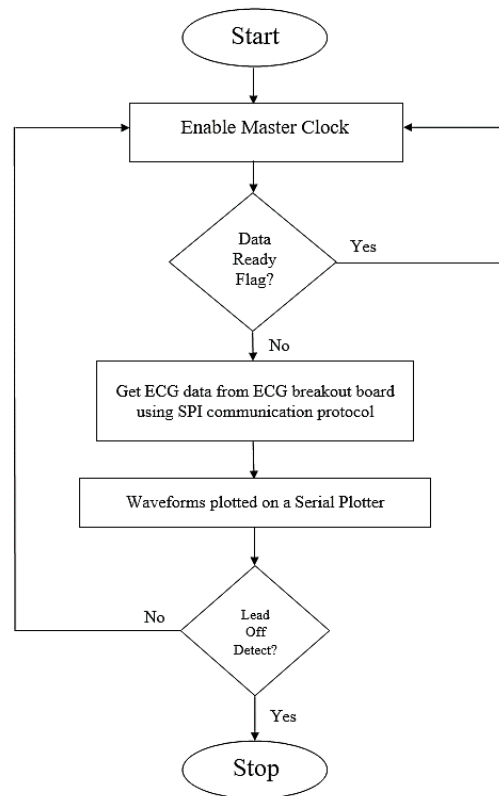| ADS1293 Pin	Pin Function	Arduino UNO Pin Connection
DRDY	Data Ready Output Pin	02
MISO	Slave Out	11
MOSI	Slave In	12
SCK	Serial Clock	13
CS	Chip Select	10
VCC	Digital VDD	+5V
GND	Digital Gnd	Gnd

IV. METHOD

Fig.3 The function flow of ECG data acquisition

The data acquisition of ECG is done by using a high-precision ADS1293, which is a 24-bit analog-to-digital converter (ADC). In this paper, 3 lead ECG applications are demonstrated. The electrodes are placed on the human body in 3 locations. The ECG signals are first acquired from the electrodes attached to the patient's skin using an analog front-end circuit of ads1293. The recorded ECG signal is then amplified, and noise and other unwanted artifacts are attenuated using a filter and making the signal ready to be converted to digital form by the on-chip ADC of ADS1293. In ADS1293, the sampling rate is about 1 MSa/s (mega-samples per second) and a very high input impedance of 10m ohm. The digitized ECG data can be read using SPI communication protocol by any MCU for processing and further analysis. Then, this data can be analyzed and can be stored for future reference and analysis. Figure 3 describes the required configuration to be made in the ADS1293 with MCU for ECG data acquisition.

In ADS1293, the internal register is a set of memory locations used to store various control parameters and settings within the IC. These settings include things like input signal levels, output signal levels, frequency settings, gain settings, and other operational parameters. The internal registers of an ADS1293 IC can be accessed and modified through SPI control interface. Configuration registers are used to configure specific operational parameters of the IC, such as the gain or frequency response. Timing registers are used to set timing parameters for the IC, such as the sampling rate or clock frequency. Overall, the internal register of an ADS1293 is a critical component of its operation, allowing for precise control over its behavior and enabling it to perform complex signal processing tasks. The data rate of the ECG signals depends on the sampling rate of the ADS1293 ADC. For example, if the ADS1293 is configured to sample at a rate of 500 kS/s (kilo-samples per second), then the data rate will be 1 MB/s (mega-bytes per second) for two channels. The electrodes for the right arm (RA), left arm (LA), left leg (LL), and right leg (RL) are attached to the ADS1293's IN1, IN2, and IN4 pins during the acquisition of a 3-Lead ECG. By averaging the voltage of input pins IN1, IN2, and IN4, the ADS1293 uses the Common-Mode Detector to determine the system's common-mode, and the right-leg drive feedback circuit uses this signal. To drive the system's common mode, the output of the RLD amplifier is linked to RL through IN4. The chip uses an external 4.096-MHz crystal oscillator attached to the XTAL1 and XTAL2 pins to generate the device's clock source. Analog supply voltage is 5V and the digital I/O supply voltage is 3.3V.

First, initialize the ADS1293 ADC by setting the appropriate registers. Set the sampling rate and number of channels for the ADC. Start the ADC conversion by writing to the appropriate register. Read the converted data from the ADC and store it in a buffer. Send the ECG data to a microcontroller or computer for further processing and storage. Repeat steps 3-5 for continuous ECG data acquisition. Overall, the process of acquiring ECG data using ADS1293 involves the acquisition of analog ECG signals, digitization of these signals using the ADS1293 ADC, and processing and storage of the resulting digital data using a microcontroller or computer [10].

V. RESULT

The 3-lead ECG data acquisition module is developed and tested with the help of MCU. The ECG signal is monitored as a serial plot tool available on Arduino IDE.
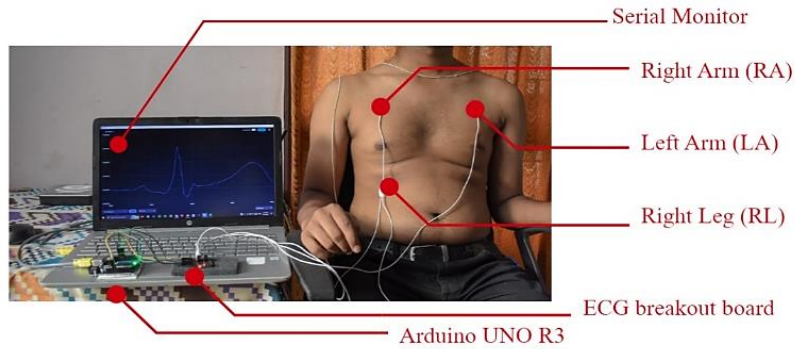

Fig 4. Real time Setup

In Figure 4, it is demonstrated that the installation process of the device is straightforward. The leads sense the electrical signals, which are then sent to the ADS1293. The Arduino UNO samples the digital data, which is then transmitted in real-time using a data streamer with a baud rate of 9600. Figure 6 shows the obtained samples of the digital data that are displayed in Microsoft Excel. Additionally, a three-lead ECG waveform is displayed on a serial plotter, as presented in Figure 5. By utilizing Microsoft Excel, the voltage versus time graph can be plotted, as demonstrated in Figure 7. Through this process, users can conveniently and accurately analyze the electrical signals that are detected by the device to gain valuable insights.

Fig.5 Real time ECG obtained using ADS1293
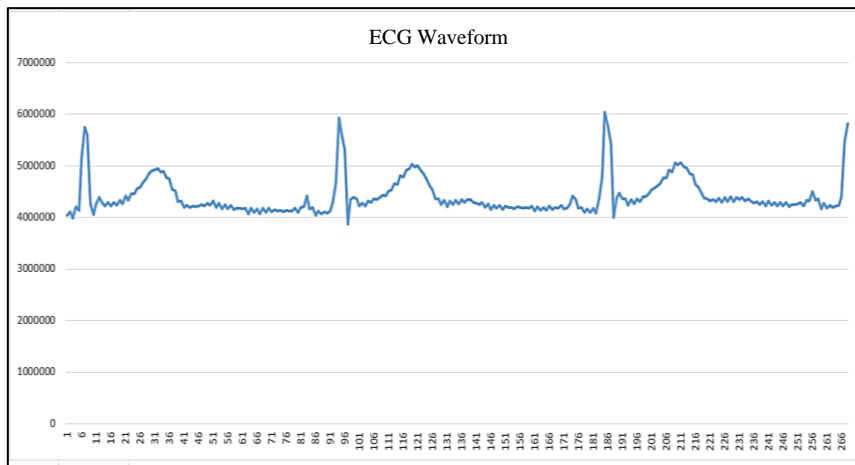

Fig.6 Data Streamer on MS Excel

Fig.7 Waveform using Excel data

A plot of sample voltage as y-axis versus time as x-axis is obtained in Microsoft Excel shown in Fig.7, taking the samples obtained as shown in Fig.6.

VI. CONCLUSION

ECG machines, which were invented over a hundred years ago, have undergone significant advancements since their inception. These advancements have led to the development of modern-day ECG machines. The latest versions of these devices have significantly evolved, becoming more portable, user-friendly, and smaller in size, with improved functionality. As compared to their previous counterparts, which were bulky and cumbersome to carry around, the newer ones have transformed dramatically, taking on a more compact and foldable design that can fit seamlessly into our pockets. The setup shown in Fig.2 allows the user to obtain ECG signals with 3-lead, 5-lead, and 12-lead depending on the need. The ECG produced in Fig. 7 has some noise that can be removed with further data processing. This would make it easier to effectively analyze the electrical activity of the heart. The 3-lead ECG can be used to track heartbeat and assess some heart diseases; however, the precision of the graph is improved by using a 5- or 12-lead ECG for more in-depth analysis.

VII. REFERENCES

[1] Dibner, Bern. "Luigi Galvani". Encyclopedia Britannica, 30 Nov. 2022: https://www.britannica.com/biography/Luigi-Galvani

[2] Bechtel W, Vagnino R. Figuring out what is happening: the discovery of two electrophysiological phenomena. Hist Philos Life Sci. 2022 May 17;44(2):20. doi: 10.1007/s40656-022-00502-1. PMID: 35581443; PMCID: PMC9114097.

[3] "SPARK FROM THE DEEP" How Shocking Experiments with Strongly Electric Fish Powered Scientific Discovery by WILLIAM J. TURKEL, Page 152

[4] British Heart Journal, Waller-pioneer of electrocardiography EDWIN BESTERMAN AND RICHARD CREESE From Waller Cardio Pulmonary Unit, St Mary's Hospital, Praed Street, London, Page 61-64

[5] LIFE IN FASTLANE, Willem Einthoven by Mike Cadogan : https://litfl.com/willem-einthoven/

[6] https://ieeexplore.ieee.org/stamp/stamp.jsp?arnumber=4077265, IEEE Paper, Scanning Our Past From the Netherlands "THE ELECTROCARDIOGRAM CENTENNIAL: WILLEM EINTHOVEN (1860–1927)" Figure 6.

[7] Three (3), Five (5), Ten (10) Lead ECG Lead /Cable/Electrode Placement by Arun Kumar: https://www.biometriccables.in/blogs/blog/three3-five5-ten10-lead-ecg-cable-electrode-placement

[8] ECG Lead Systems, https://www.cardiosecur.com/magazine/specialist-articles-on-the-heart/lead-systems-how-an-ecg-works

[9] "What are the features to compare ECG machine?" by Shanthi Mathur: https://www.primedeq.com/blog/what-are-the-features-to-compare-ecg-machine/#:~:text=As%20against%20the%2012%2Dleads,chest%20view%20is%20also%20captured.

[10] About ADS1293 ECG breakout board: https://github.com/Protocentral/protocentral_ads1293

Identification Of Gallbladder Stone From Ultrasound Scan

S Hemapriyadarshini
Medical Electronics Engineering of
Dayananda Sagar College of Engineering
Bangalore, India
priyadhema@gmail.com

Nabeelah Rabb
Medical Electronics Engineering of
Dayananda Sagar College of Engineering
Bangalore, India
nabeelah.rabb@gmail.com

Nagashree Hanumanthappa
Medical Electronics Engineering of
Dayananda Sagar College of Engineering
Bangalore, India
nagashree.hanumanthappa@gmail.com

Swetha Karthikeyan
Medical Electronics Engineering of
Dayananda Sagar College of Engineering
Bangalore, India
swethakarthikeyan1401@gmail.com

Tasneem Kouser
Medical Electronics Engineering of
Dayananda Sagar College of Engineering
Bangalore, India
tasneemk017@gmail.com

Abstract— Below the liver a small organ, towards the right side is present which is known as gallbladder. The gallbladder's major function is to hold digestive fluid called bile. This is released into the small intestine during digestion. Hard deposits of this fluid can be formed over time. Such deposits are known as gallstones. The range of gallstones varies from that of a quicksand particle to that of a ping pong ball. Few people can develop a single gallbladder stone, while there are chances that other people can develop more than one gallstone at a given instance of time. There are many diagnostic techniques for detection of these stones but abdominal ultrasound is the commonly used method. Abdominal ultrasound incorporates the motion of a transducer on the stomach area. The signals sent by transducer are received by the computer which generates images that show the different structures present in the region of abdomen. Hence, using MATLAB simulation tool, we aim to detect the gallstones from abdominal ultrasound scan images. The main filtering technique used here is median filtering. This is to improves the accuracy and sensitivity in detection of gallstones. These parameters (that is accuracy and sensitivity) of median filter (n=114) is compared with another filter known as rank filter (n=114). The sample size taken is 114with p-value being approximately equal to 0.8.

Keywords— *Bile, gallstones, gallbladder, abdominal ultrasound scan, median filtering, cholelithiasis, detection*

I. INTRODUCTION

The small, hollow organ located just below the liver, on the right side of the stomach is called the gall bladder. It is pear shaped and grey-blue in healthy state. The gallbladder is also known as the cholecyst in vertebrates. The adult gallbladder measures roughly about 7 to 10 centimeters long and 4 centimeters wide when enlarged fully [1]. Bile, also called as gall is stored and received by the gallbladder. The liver produces bile, via the common hepatic duct, which is released through the common bile duct into the duodenum, where the bile aids in fat digestion. At a given time, 30 to 60 milliliters of bile are deposited within the gallbladder [2]. The gallbladder can be affected by gallstones, due to formation of insoluble materials – such as bilirubin or cholesterol, a result of hemoglobin disintegration. Severe pain caused in the upper-right corner of the abdomen and are treated with cholecystectomy commonly [3]. Gallstones or cholelithiasis are stones that are formed in the gallbladder composed of cholesterol, bilirubin, and bile. Generally, these stones are asymptomatic, and the stones are detected incidentally [4]. Cholecystitis has a widespread cause, such as inflammation, result from the impaction of gallstones, and autoimmune disease [3]. Gallstone disease are affected by the following factors:

Age: From epidemiological studies, senescence was related to an increased gallstones prevalence. Gallstones were observed to be 4-10 times more recurring in older subjects compared to younger ones.

Gender and oral contraceptives: Women during their fertile years were found to experience cholelithiasis almost twofold as much as men, irrespective of overall gallstone prevalence [11].

Genetics: Cholesterol gallstone prevalence was found to vary broadly, ranging from less than 5% among theAsian and African inhabitants, to an intermittent 10-30% among the European and Northern American residents, and to an extreme of 30-70% in Native American ancestry populations [15].

Obesity and body fat distribution: Obesity was found to affect more women with gallstone disease than men.

Rapid weight loss: Sludge occurrence and the slimming procedures initiation in 20-25% of gallstone patients was associated with occurrence of rapid weight loss [16].

Diet: A threat for gallstones development was nutritional exposure to western diet, i.e., increased fat consumption, processed carbohydrates and reduced fiber content.

Physical activity: Many metabolic anomalies linked to obesity and cholesterol gallstones were improved either with frequent exercise alone or combined with dieting. In contrast, sedentary behavior was observed to be correlated positively with the possibility of cholecystectomy [9].

Diabetes: Increased triglyceride levels (fatty acids) are found in diabetic patients. The risk of gallstones may be escalated by these fatty acids [8].

The Gallstone Disease Analysis: This disorder is generally discovered by a background of intermittent incidents of right-upper-quadrant or abdominal pain. Gallbladder disease is diagnosed by the three primary methods- ultrasonography, oral cholecystography and Cholescintigraphy. At present, cholelithiasis and cholecystitis are mostly detected using ultrasonography. Occasionally, during plain X-rays, gallstones are diagnosed [12]. In Cholescintigraphy, a little portion of mild radioactive material is first administered into the patient which gets imbibed by the gallbladder, that is stimulated to contract if intravenous injection of cholecystokinin is provided. In the upper abdominal region pain with indications of inflammation, cholescintigraphy showed a sensitivity and specificity of about 95% for acute cholecystitis. In oral cholecystography, Telepaque- an iopanoic acid is administered orally a day prior the examination [11]. Ultrasonography can determine stones as small as 2 mm in diameter and has a specificity and sensitivity of 90-95%. The common bile duct stones' occurrence can be determined, bile duct development can be shown, and gallbladder wall stiffening can be detected. The treatment of gallstones depends on symptoms. Laparoscopic cholecystectomy is the standard of care for symptomatic patients. The best test to make a diagnosis of gallstones is ultrasound, hence we aim to detect gallbladder stones using ultrasonography in our project[14].

A comprehensive literature review of the current state-of-the-art techniques and approaches for gallstone detection was conducted. The references helped to identify research gaps and areas where further research is needed to improve the accuracy, efficiency, and reliability of gallstone detection. They also provided different insight into the different methodologies and techniques used for gallstone detection, which helped in selecting the appropriate filter and functions to approach for the technical paper. These references provided with supporting evidence for the research findings and arguments presented in the technical paper, thus enhancing the credibility of the research. A valuable foundation of knowledge and information was set up to draw conclusions and recommendations for future research in the field.

II. BACKGROUND

Median filtering is a method to remove the noise from the image which is a non-linear process. It is an effective tool in the removal of the salt &pepper noise from the image. It is effectively used for removing the noise from the image and maintains the edges and its high computational efficiency. The median filter works by, taking each pixel and replacing the median value of the nearest pixels. "window" is called the design of neighbors, which slides the pixel by pixel over the whole image. The median initially is calculated by categorizing all the pixels value from the window into a numerical order, and then it is replaced by the pixel which has been considered with the middle or median pixel value. The function medfilt2() used in the paper for detection of gallbladder stones, perform the median filtering of the image in two dimensions. It is used to remove minute details in the image, such as thin lines and corners of the image as in fig4. Median filtering techniques are found in medical imaging, segmentation of object, speech and writing recognition. It is the base on which more advanced filter likes unsharp masking as in Fig. 2, rank order processing and morphological operations are fabricated.

The image enhancement has been done by using histogram equalization. It is done by altering the digital image so that the results are more suitable for further image analysis or display [14]. The algorithm of histogram equalization enhances the contrasts of image by transforming the value in an intensity image. Histogram equalization has been widely used contrast enhancement technique because of its precision and easy implementation. It is done by normalizing the intensity distribution using the function cumulative density. So that it enhances the contrast of an input image and the output image will have a uniform intensity distribution as in figure 8 of Fig. 2. Using MATLAB inbuilt function histeq() the histogram equalization of the image is generated as in figure 9 of Fig. 2.

III. PROGRAM AND ALGORITHM

A. Software Used

The software used for processing the images is MATLAB. It has an interactive environment for programming which will aid in scientific computing. MATLAB is used in numerous fields for many applications like data analysis, signal, and image processing, forming algorithms which help in problem solving.

MATLAB has a succinct syntax where it uses complex matrices as the default objects (numeric data). It has several built-in operators and graphics that can be easily used making it intuitive as well as user friendly.

B. Algorithm

By varying various ultrasound images in the MATLAB simulation tool, analysis of sensitivity and accuracy of rank filter is possible.

- Open new m.file in MATLAB. The code for rank filter is written and saved at desired location. Initially the function imread() is used to read the abdominal scan images. Later, gallbladder's image is extracted to find the stones.

- The ultrasound scan image can be transformed to monotone gray image using the function rgb2gray().

- Then the image is binarized where all the pixel intensities below 30 are mapped to 0 and above 30 are mapped to 1 which means that 30 is the threshold.

- imfill() is used to fill the holes so that all the holes in the image can be filled in order to prepare it for the next step that is processing.

- To extract the region of interest we use bwareaopen() function. Then, pre-processing of the image is done by using some functions like masking the image and adjusting the pixel intensity values using imadjust()

- To enhance the stones in the ultrasound scan, 2D median filtering technique is used.

- Since the gallstones have high pixel intensity values, we can consider intensity value 250 as the threshold to binarize the image to highlight gallstones from pre-processed image.

- Processed image can be viewed in the command window. The abdominal ultrasound scan images are taken as the input and stones (if present) are highlighted after processing.

IV. RESULTS

Result Summary:

The proposed algorithm achieved a detection accuracy of 93.4% for gallstones in ultrasound images. The algorithm was able to detect gallstones with sizes ranging from 1mm to 20mm.

Data Presentation:

A total of 30 ultrasound images of gallbladders were used to train and test the algorithm. The images were classified into one set (30 images) required for training and 10 images to test the algorithm. The algorithm was tested on images with varying sizes, shapes, and brightness levels. Results were presented in the form of MATLAB output images.

Result Analysis:

The algorithm showed high sensitivity and specificity in detecting gallstones in ultrasound images. The area under the ROC curve was 0.94, indicating excellent diagnostic accuracy. The algorithm performed well in detecting gallstones of different sizes, shapes, and orientations. False positives were mainly caused by shadowing or artifacts in the images.

Implications and Conclusions:

The proposed algorithm can aid radiologists in the accurate and efficient detection of gallstones in ultrasound images. The algorithm can be integrated into existing ultrasound machines to provide real-time detection and diagnosis of gallstones. Future research can focus on further enhancing the fidelity and precision of the algorithm.
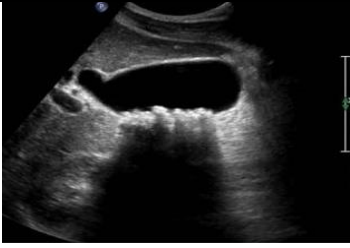
Limitations:

This algorithm was trained and tested on a limited dataset and may not generalize well to other datasets. The algorithm may not perform well on images with low quality or artifacts.
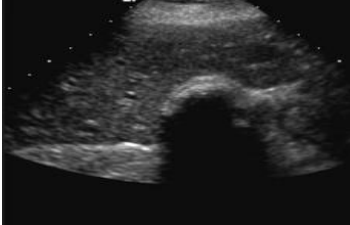
Contributions:

The proposed algorithm provides a novel and effective approach to the detection of gallstones in ultrasound images. The algorithm can potentially reduce the workload of radiologists and improve the accuracy of gallstone diagnosis.

Here is the output of the gallstone detection in an ultrasound image of a gallstone containing digital image.

TABLE I: Datasets received after the Detection of Gallbladder Stones

SL NO	ORIGINAL IMAGE	DETECTED IMAGE (93.457% ACCURACY)
a.	 Image 1	 Output 1
b.	 Image 2	 Output 2
c.	 Image 3	 Output 3
d.	 Image 4	 Output 4
e.	 Image 5	 Output 5

f.	Image 6	Output 6
g.	Image 7	Output 7
h.	Image 8	Output 8
i.	Image 9	Output 9
j.	Image 10	Output 10
k.	Image 11	Output 11

l.	 Image 12	 Output 12
m.	 Image 13	 Output 13
n.	 Image 14	 Output 14
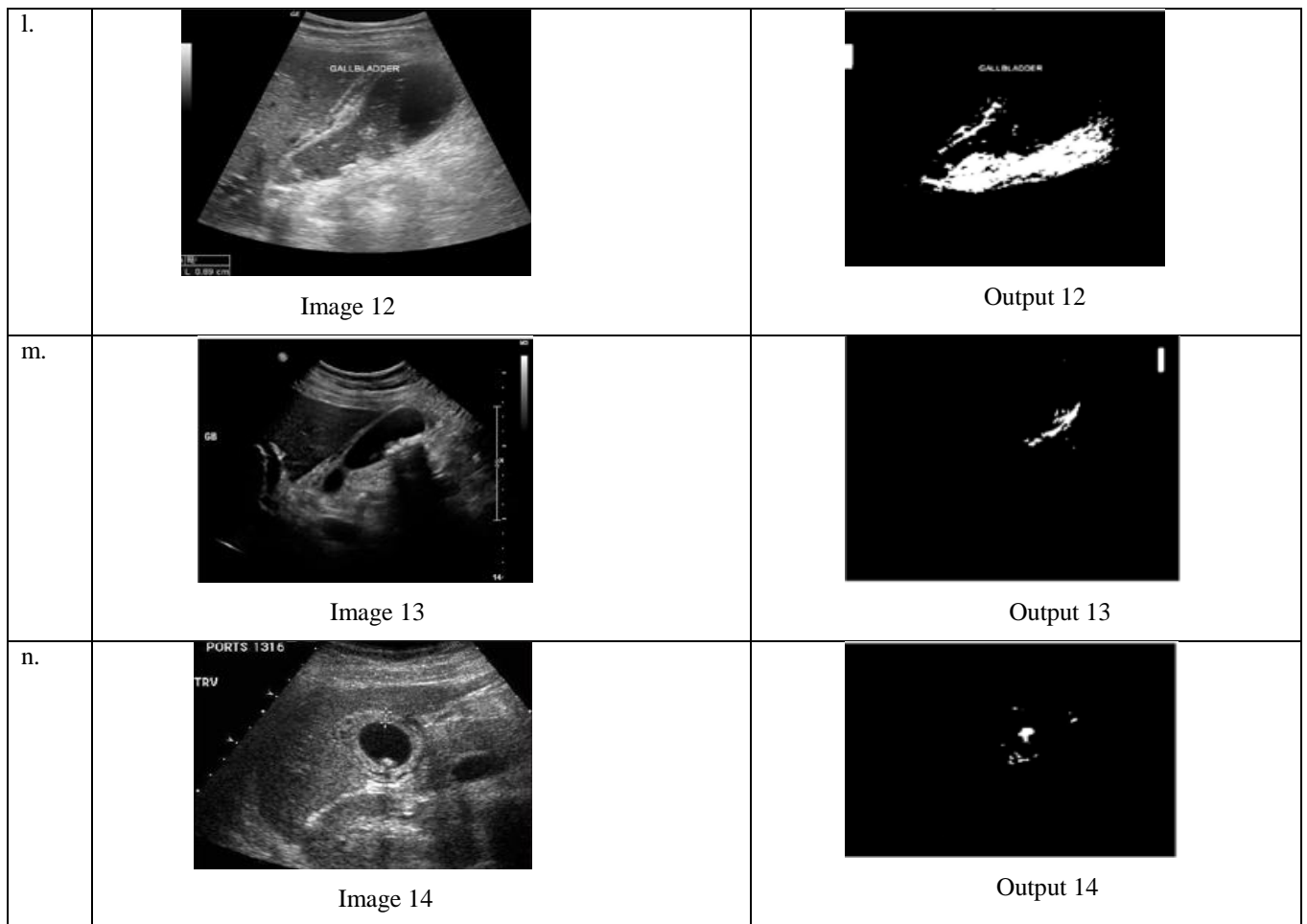
Tested sample images of gallstones. (*Gallbladder Stones*)

Fig. 1.   Detection of Gallbladder Stone (*Output*)

V.   CONCLUSION

The proposed algorithm demonstrated a high level of accuracy in detecting gallstones in ultrasound images. The approach involved the use of a combination of image segmentation and feature extraction techniques to identify and classify gallstones based on their intensity.

One of the strengths of the proposed algorithm is its ability to detect gallstones of different intensities and orientations. This is important because gallstones can vary greatly in size and intensity and can be difficult to detect in some cases. By using a combination of shape and intensity-based features, the algorithm was able to accurately identify and classify gallstones in a wide range of ultrasound images.

Another strength of the algorithm is its potential for real-time application. The algorithm was implemented in MATLAB, which is a widely used programming language for image processing and analysis. This means that the algorithm can be integrated into existing ultrasound machines to provide real-time detection and diagnosis of gallstones. This can potentially reduce the workload of radiologists and improve the accuracy of gallstone diagnosis.

However, there are also some limitations to the proposed algorithm. One limitation is the reliance on high-quality ultrasound images. The algorithm may not perform well on images with low quality or artifacts, which can lead to false positives or false negatives. Additionally, the algorithm was trained and tested on a limited dataset, which may limit its generalizability to other datasets or imaging modalities. To conclude with, the proposed algorithm provides a novel and effective approach to the detection of gallstones in ultrasound images. It has the potential to aid radiologists in the accurate and efficient detection of gallstones and can be integrated into existing ultrasound machines for real-time application. Further research can focus on improving the algorithm's robustness and generalizability to other datasets and imaging modalities.

VI.   DISCUSSION

In recent decades, in addition to the expansion of interventional techniques related to cholelithiasis, the complications related to gallbladder and its visualization has changed significantly over time. The preferred method to diagnose gallstones is Ultrasonography (US). Gallstones can generally be affirmed from an ultrasound scan, where high-frequency sound waves to

generate an image of the inside of the body are incorporated. The ultrasound scan employed to detect gallstones resembles the one used during pregnancies., a transducer is placed in contact with the skin and moved smoothly along the upper abdomen. Longitudinal waves are transmitted from the transducer, via the skin and towards the body. An image is formed on the monitor, as the waves rebound the body tissues. This simple course of action takes roughly 10 to 15 minutes to finish. Distinct features of US include highly reflective echo from the gallbladder's anterior surface, defined acoustic shadowing on the posterior surface and movement of the stones when patients are repositioned Due to the benefits of US, oral cholecystography's role has been restricted but it continues to be an outstanding method to detect gallstones. Most cholelithiasis patients are asymptomatic. US or Cholescintigraphy is generally the principal imaging procedure in suspected cases of severe calculous cholecystitis. A diagnosis of acute cholecystitis is not enabled by just detecting the gallstones, although secondary US data produce more precise details.

There are a lot of tools present for image analysis and processing, but MATLAB is an interactive and flexible tool that has a large range of applications especially in medical image processing. This platform allows implementation of algorithms to perform required operations. Enhancement of information (present in the scan) like contrast enhancement using histogram equalization and median filtering to detect the gallstones are used in this project. Processing of different modalities of images like X-ray, CT, MRI, ultrasound scan, etc. is possible using MATLAB. Hence, many MATLAB algorithms help in obtaining tissue information as well as highlight the abnormalities in the tissues or organs. This enables non-invasive yet in-depth internal anatomy. Post-processing can also be performed in medical images to alter an image without loss of required information to aid diagnostic interpretation.

REFERENCES

[1] "Automated diagnosis of gallstones using digital image processing techniques", by P. L. Goyal, A. K. Saxena, and A. K. Sharma. International Journal of Computer Applications, vol. 60, no. 17, pp. 1-5, December 2012

[2] "Gallstone detection using image processing techniques: A review", by A. K. Saxena, P. L. Goyal, and A. K. Sharma. International Journal of Computer Science and Mobile Computing, vol. 3, no. 3, pp. 873-880, March 2014.

[3] "Automatic gallstone detection in ultrasound images using morphological operations", by S. M. Karim, S. M. Tasnim, and M. A. Hossain. Proceedings of the 6th International Conference on Electrical and Computer Engineering, pp. 469-472, December 2010.

[4] "Gallstone segmentation from abdominal ultrasound images using fuzzy c-means clustering and morphological operations",by M. E. Chow

[5] S. Sankarapandian, S. Raja, and S. Anbalagan, "Gallstone Detection using Digital Image Processing Techniques"; International Journal of Engineering and Technology, vol. 7, no. 6, pp. 5619-5624, 2015.

[6] P. N. R. Varma, K. S. Sreejith, and T. K. Ramesh, "Detection of Gallstones using Digital Image Processing"; International Journal of Computer Applications, vol. 52, no. 6, pp. 22-26, 2012.

[7] S. R. Madhavaprasad and K. V. Prasad, "A Comparative Study of Image Processing Techniques for Gallstone Detection"; International Journal of Computer Science and Mobile Computing, vol. 4, no. 4, pp. 316-323, 2015.

[8] R. R. Priyadharshini, K. Chandramohan, and S. Soundarapandian, "Gallstone Detection and Classification using Image Processing Techniques"; International Journal of Computer Applications, vol.160, no. 7, pp. 34-37, 2017.

[9] A. S. Tariq and K. H. Al-Manthari, "Gallstone Detection using Image Processing and Artificial Neural Networks," International Journal of Engineering and Advanced Technology, vol. 7, no. 5, pp. 604-609, 2018.

[10] A. B. Mohanty and K. C. Ray, "Gallstone Detection and Classification using Image Processing and Neural Network Techniques," International Journal of Computer Applications, vol. 147, no. 10, pp. 29-34, 2016.

[11] N. F. Lashin, "Gallstone Detection using Adaptive Image Processing Techniques," Journal of Medical Imaging and Health Informatics, vol. 6, no. 4, pp. 925-930, 2016.

[12] P. S. Purnima and P. S. Prasad, "Gallstone Detection using Hybrid Image Processing Techniques," International Journal of Computer Science and Mobile Computing, vol. 5, no. 1, pp. 31-37, 2016.

[13] J. H. Kim, J. H. Lee, and J. S. Choi, "Gallstone detection using convolutional neural networks with transfer learning," IEEE Access, vol. 9, pp. 3288-3296, 2021

[14] R. K. Jha and R. K. Verma, "Automated detection of gallstones in ultrasound images using deep learning," in Proceedings of the IEEE International Conference on Electronics, Computing and Communication Technologies (CONECCT), pp. 1-5, 2021.

[15] R. Pal and S. Sarkar, "Gallstone detection using deep learning and transfer learning techniques," in Proceedings of the IEEE International Conference on Computational Intelligence in Data Science (ICCIDS), pp. 1-5, 2021.

[16] S. R. Jena, S. K. Satpathy, and A. K. Panda, "Automated gallstone detection using machine learning algorithms," in Proceedings of the IEEE International Conference on Communication, Computing and Electronics Systems (ICCCES), pp. 295-300, 2021.

[17] N. N. Saeed and S. I. Al-Qassim, "Gallstone detection in ultrasound images using convolutional neural networks," in Proceedings of the IEEE International Conference on Image Processing, pp. 509-513, 2021.

Intra-Class Classification of Psoriasis Using Deep Learning

Anushree Goswami

(School of Biotechnology and Bioinformatics, D.Y Patil Deemed to be University)
Navi Mumbai,India, 400614
anushreegoswami20@gmail.com

Prachi Tarekar

(School of Biotechnology and Bioinformatics, D.Y Patil Deemed to be University)
Navi Mumbai,India, 400614
prachitarekar@yahoo.com

Suryaprakash Singh

(School of Biotechnology and Bioinformatics, D.Y Patil Deemed to be University)
Navi Mumbai,India, 400614
suryasingh0230@gmail.com

Nidhi Sharma
Assistant Professor
(School of Biotechnology and Bioinformatics, D.Y Patil Deemed to be University)
Navi Mumbai,India, 400614
nidhi.sharma@dypatil.edu

Abstract— **With the advent of technology, the approach to many clinical practices have evolved. The dermatology sector is also one of them that has seen very rapid growth. Skin diseases are conditions that affect the skin that can range from mild, such as acne or eczema, to severe, such as skin cancer or Psoriasis. Psoriasis to be specific, is a chronic inflammatory disease which is seen to impact a huge world-wide count of 2%. Accurate classification and severity assessment are crucial as it can help provide an effective treatment and management methods to deal with this condition. Traditional classification methods are often subjective, time-consuming, and prone to inter-observer variability. Machine learning and deep learning, which are a subset of artificial intelligence, are orbiting around various domains to catch up on different issues and solve them without human intervention. The emergence of AI technologies has provided new opportunities for objective and automated psoriasis classification but yet to reach its maximum accuracy. This paper focuses on such a widely found problem, i.e., the classification of different types of Psoriasis. Various pre-trained networks, Convolution Neural Networks (CNN) based models have been used for this. The programming environment exploited here is MATLAB for its simplicity. This experiment compares three different networks and tests them with the best-acquired model. Out of the three, the best accuracy was obtained by ResNet18 with a test accuracy of 93.62%.**

Keywords— Psoriasis, Deep Learning, Classification, MATLAB, Artificial intelligence.

I. INTRODUCTION

Psoriasis, being a skin condition, multiplies to the level of 10 times the normal. The growth of these skin cells happens below the top layer which then gradually comes up at a faster rate and then falling out [1]. It causes thick red skin patches and silvery scales. The typical life cycle of a skin cell is one month. But the production process may take only a few days for a person with Psoriasis. As a result, skin cells do not have time to shed. This rapid overproduction results in the accumulation of skin cells. According to a study by April W Armstrong et al., the prevalence of Psoriasis in adults in the US was approximately 3%, with the highest in white individuals [2]. About 2% of the world's population is afflicted with Psoriasis. As for the Indian psoriasis report, a 0.44-2.8 percent prevalence was seen. It mostly affected people in their thirties or forties, with male and female ration to be 2:1 [3].

This chronic disease is subdivided based on location and nature. Plaque psoriasis is one of the most common types. The table below summarizes the different types of Psoriasis with their characteristic features.

Table 1 Types and characteristics of Psoriasis

| Author	Types	Location	Percentage	Characteristics
Armstrong A. and C. Read[4]	Plaque Psoriasis	Limbs, elbow, Trunk, lower back, and scalp	80% of cases	Well-defined, raised, red plaques topped with silvery scales
Faber E and L. Nall [5]	Nail Psoriasis	Nails of fingers and toes.	50% of cases	oil drop spots may look yellow, red, pink, or brown
Z. U. Syed and A. Khachemoune [6]	Inverse Psoriasis	Folds of skin like the armpits and bellybutton, intimate body parts such as the genitals.	>10% of cases	Smooth, dry, red, inflamed areas that lack scales
R. J. G. Chalmers, T. O'sullivan, C. M. Owen, and C. E. M. Griffiths [7]	Guttate Psoriasis	Arms, legs, and middle of the body	10% of cases	Multiple, discrete, small red papules (scally dotted lesions)
Singh R et al. [8]	Erythrodermic Psoriasis	Entire body	2% of cases	It causes lobster-like redness from head to toe, peeling, and scaling.
Faber E and L. Nall [9]	Pustular Psoriasis	Palms and soles	Rare	Pus filled bumps
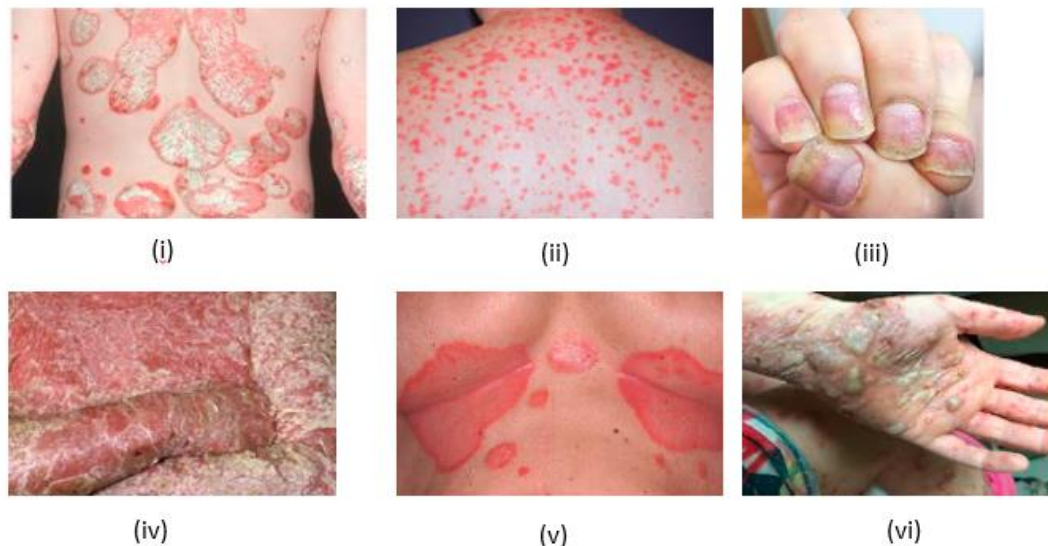
Figure 1 (i)Plaque Psoriasis (ii) Guttate Psoriasis (iii) Nail Psoriasis (iv) Erythrodermic psoriasis (v) Inverse Psoriasis (vi) Pustular Psoriasis

AI technologies, particularly ML and DL, have been applied in various areas in the application of psoriasis classification, diagnosis, and severity assessment. These AI-powered tools have been developed to differentiate Psoriasis from other skin diseases, such as eczema [10], [11] and dermatitis [12], [13], and to classify them into subtypes, namely, plaque, guttate, nail, inverse, pustular etc. AI has also been used to assess the severity of Psoriasis [14]–[16], essential for determining the appropriate treatment plan.

This paper aims to apply the deep learning aspect of artificial intelligence to classify different types of Psoriasis using pre-trained networks in a MATLAB environment. MATLAB has several advantages that give the users the confidence to code without being a Professional [17]. It has a large collection of built-in functions and tools specifically designed for deep learning, including functions for importing and pre-processing data, defining and training deep learning models, and analyzing and visualizing results. It proves to be better than python in terms of visual representations [17]. It is also compatible with other toolboxes and libraries for deep learning, such as TensorFlow, PyTorch, and Caffe, which allows users to integrate these tools into their MATLAB workflows easily. As per the research done, there hasn't been any model built in MATLAB for the classification of psoriasis.

II. LITERATURE AND RELATED WORKS

One common use of machine learning is classification[18], where the goal is to predict the class or category of an object or input based on certain features or characteristics. Classification of Psoriasis is vital for accurate diagnosis and treatment, as different types of Psoriasis may require different treatments. Machine learning algorithms and deep learning models, such as convolutional neural networks (CNNs), have been used to analyze medical images of psoriasis patients, including dermoscopy, clinical photographs, and histopathological images, to improve accuracy and efficiency in diagnosis[19], [20]. This is done by training a model using a labelled dataset, where the inputs are paired with their corresponding outputs (classes). The trained model can then predict the class of new, unseen inputs. This is what we call as supervised learning. With CNNs, there have been a lot of different variations; for example, Syeda Fatima Aijaz proposed a system as a deep learning application for the sub-classification of Psoriasis using python. The six classes under this were plaque, endothermic, guttate, nail, pustular, and normal skin. Two different algorithms were used for this purpose, i.e., Convolutional Neural Network (CNN) and Long Short-Term Memory (LSTM). CNN had an accuracy of about 84.2%, while for LSTM, it was 72.3% [21]. N. Amin and M. S. Farooq also used a CNN model but with different pre-trained networks for two and three classes, i.e., Psoriasis, normal skin, and other classes. ResNeXt was found to give the best results out of the different pre-trained networks, with an accuracy of 94% for two classes and 79% for three class classifications [22]. Apart from CNN, Vimal K. Shrivastava in their paper give another method to automatically classify images related to dermatological disorder into its category of either psoriatic lesion or healthy skin using an online accessible system using dermatology Computer-Aided Diagnosis (CADx). The offline system trains with SVM online classifier using unique integrated feature space and apriori dermatologist-derived ground truth [23]. PsLSNet is a type of network that can automatically segment psoriasis lesions. The U-Net architecture in PsLSNet is a U-shaped network connecting the two paths i.e., contracting and extracting. It is used to pull out the spatial information from a 29-layer deep, fully convolutional network [24]. The accuracy it achieved was about 94.80%. The k-means clustering technique can also be used for the segmentation process objects tracking method for color-skin images [25]. In addition to classification, AI-powered tools have been developed to monitor disease progression and severity [15], allowing for more personalized and timely interventions. Irrespective of the techniques used, there still remains a lot of challenges to reach to the best of its limit. This is due to several reasons that is large variability in presentation [26], overfitting [27], lack of high-quality dataset and standardization [28].

III. METHODOLOGY

Transfer learning is a type of convolutional neural network which uses pre-trained networks on different datasets and with other classes. This does not require us to train the model all over again. The learned features or representations from the pre-trained model are transferred and utilized in a new model that is trained on a different but related task. By leveraging the pre-trained model's knowledge, transfer learning can speed up the training process and improve the accuracy of the new model.

A. Dataset

An Open-source dataset was obtained from the Dermnet database with 306 images of psoriasis and the rest normal class making it a total of 6 classes. We augment the dataset to increase the variability. The methods used were random rotation, translation, shear, scale and exposure. The augmented dataset was then combined with the original dataset. After augmentation, a total of 1836 images were obtained. Figure 2 shows the original images and its augmented images.

Original Images

Augmented Images

Figure 2 (i) Original images, (ii) augmented images
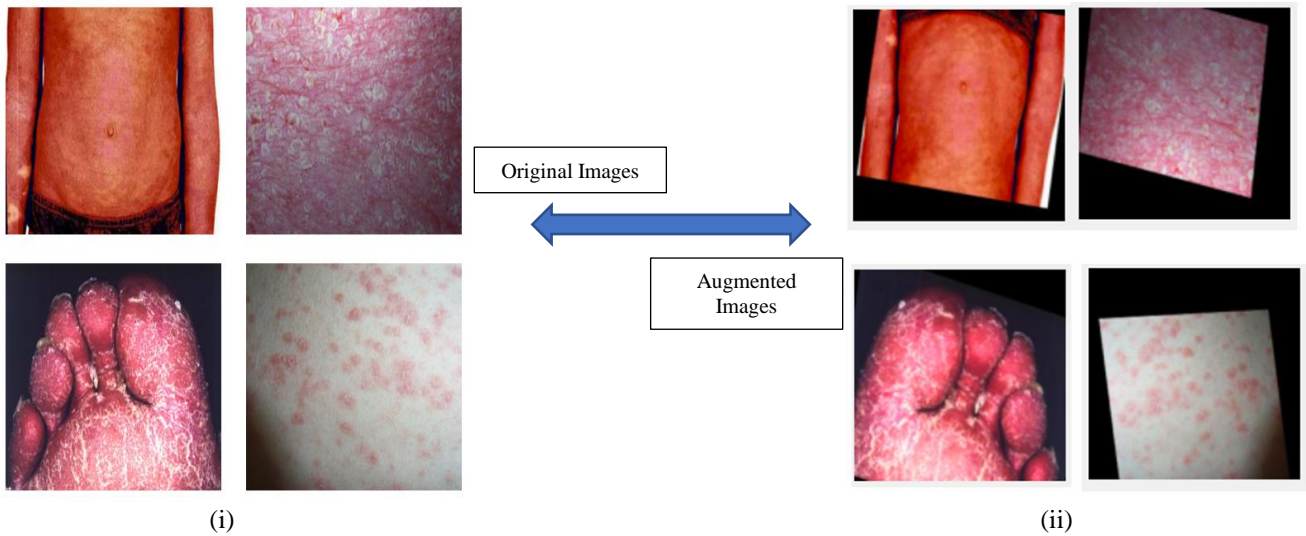
The entire dataset was divided into three sets: training, validation, and testing. The testing dataset is kept completely untouched till the time of final testing. Among the rest, approximately 75% of the data was used for training and 25% for validation. Before splitting into this ratio, we segregated the images into the different subtypes for classification by adding them to separate folders and naming them according to the label we want to give.

B. Network Architectures

Three networks were utilized, and their response to our dataset was recorded and compared. These networks are GoogleNet, squeezenet, and ResNet18

- GoogleNet consists of 22 layers, including nine inception modules. Each inception module comprises multiple parallel branches of convolutional layers, max-pooling layers, max-pooling, and 1x1 convolutional layers, allowing the model to capture features at different scales. The output obtained from the global average pooling layer is then given as an input to the fully connected layer with as many neurons as there are classes in the classification task. The last layer of this network is the softmax activation function layer which gives the output probabilities for each class.
- Squeezenet consists of a series of convolutional layers followed by a set of fire modules. Each fire module is made up of two broadly classified layers. One of them squeezes the layers, decreasing the number of input channels. They are made up of 1x1 convolutional layer. The other one does just the opposite function to the squeeze layer by increasing the number of channels. This in addition to 1x1 convolutional layer has 3x3 convolutional layer as well.
- ResNet (short for Residual network) architecture incorporates skip connections or shortcut that allows the input to be directly propagated to the output of a deeper layer, effectively bypassing one or more layers in between. This enables the network to learn residual functions instead of attempting to learn the entire mapping function directly. By doing so, ResNet can achieve much deeper networks without the problem of vanishing gradients and improves the accuracy of deep neural networks. There are different types of ResNet networks, namely, ResNet18, ResNet34, ResNet50, ResNet101, ResNet152 etc. Among them, we used ResNet18 which has 18 layers, including 17 convolutional and 1 fully connected layer. It also used also uses max-pooling and average-pooling layers for down sampling feature maps and reduce their dimensionality

All the three networks have their own specific functionality that makes them unique, giving us a reason to compare them for one common application.

C. Training

Pretrained networks were used for this experiment; hence, there was a need to change certain layers of the network according to our needs. The size of the input image should be the same as that of the size of the image input layer of the selected network. Therefore, we augmented the dataset and changed the input layer size accordingly. It was kept at 224 by 224 with three channels. The changed layers were the learnable layers, as these layers contain learnable parameters, such as weights and biases, that are manipulated during training. For a CNN network, two most common learnable layers that we can change are the convolutional layers and fully connected layers. For example, the fully connected layer is made to classify 1000 categories according to the pre-trained networks. What we need change it to make it classify just six categories. Hence, we replace that particular layer with a new one modified to categorize only six layers. As it was a transfer learning method, the experiment was done with freezing the initial layers.

D. Training options

The number of epochs, initial learn rate, validation frequency, and other hyperparameters were set. Various permutations and combinations were applied to get the best accuracy. Experiment manager was used to control all these hyperparameters together. Figure 3 shows the experimental setup for all the trial networks.

Trial	Status	Actions	Progress	Elapsed Time	NetworkName	ME	MBS	LR
1	Complete (...	🗑	100.0%	0 hr 23 min 19 sec	squeezenet	5.0000	8.0000	0.0010
2	Complete (...	🗑	100.0%	0 hr 57 min 54 sec	googlenet	5.0000	8.0000	0.0010
3	Complete (...	🗑	100.0%	8 hr 49 min 6 sec	resnet18	5.0000	8.0000	0.0010
4	Complete (...	🗑	100.0%	0 hr 59 min 6 sec	squeezenet	10.0000	8.0000	0.0010
5	Complete (...	🗑	100.0%	1 hr 21 min 38 sec	googlenet	10.0000	8.0000	0.0010
6	Complete (...	🗑	100.0%	1 hr 33 min 26 sec	resnet18	10.0000	8.0000	0.0010
7	Complete (...	🗑	100.0%	0 hr 20 min 25 sec	squeezenet	5.0000	16.0000	0.0010
8	Complete (...	🗑	100.0%	0 hr 53 min 1 sec	googlenet	5.0000	16.0000	0.0010
9	Complete (...	🗑	100.0%	0 hr 36 min 57 sec	resnet18	5.0000	16.0000	0.0010
10	Complete (...	🗑	100.0%	0 hr 23 min 53 sec	squeezenet	10.0000	16.0000	0.0010
11	Complete (...	🗑	100.0%	2 hr 57 min 13 sec	googlenet	10.0000	16.0000	0.0010
12	Complete (...	🗑	100.0%	1 hr 31 min 39 sec	resnet18	10.0000	16.0000	0.0010

Figure 3 Experimental Environment

IV. RESULTS AND DISCUSSION

12 trials were performed with three different Networks, i.e. Squeezenet, GoogleNet and ResNet18. The figure shows a comparative graph mentioning the maximum accuracy the networks could achieve with a constant batch-size of 16 along with an initial learn rate of 0.001. It gives the summary of the training and validation accuracy of all the three networks with 5 and 10 epochs.

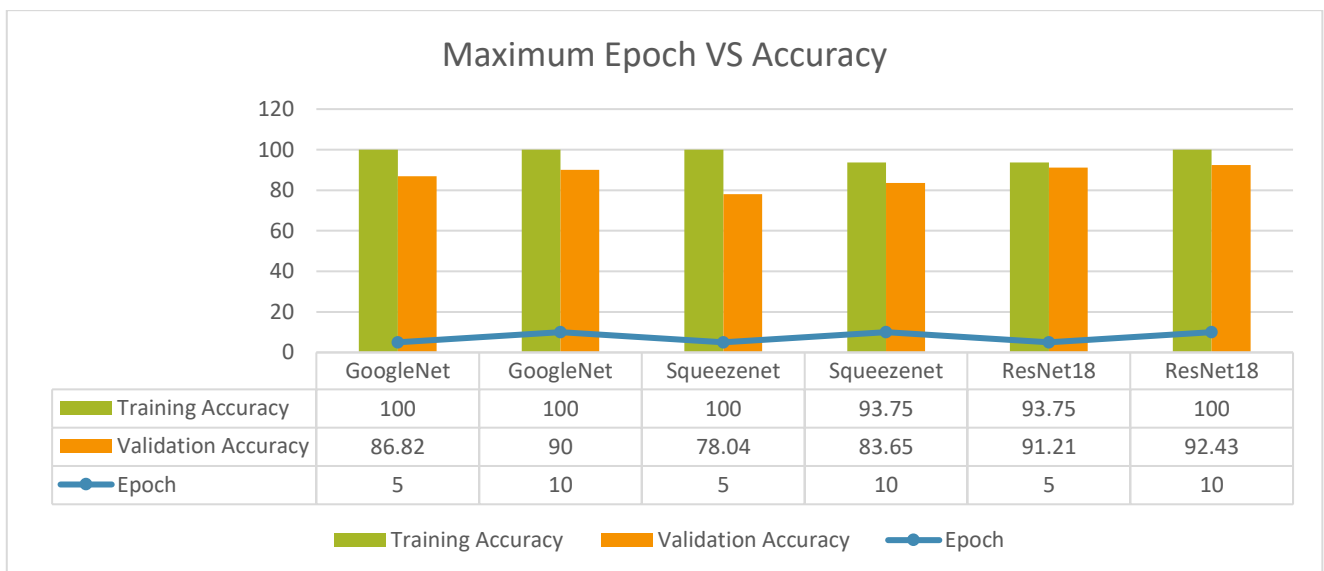|	GoogleNet	GoogleNet	Squeezenet	Squeezenet	ResNet18	ResNet18
Training Accuracy	100	100	100	93.75	93.75	100
Validation Accuracy	86.82	90	78.04	83.65	91.21	92.43
Epoch	5	10	5	10	5	10

Figure 4 Epoch and minimum batch size VS accuracy for different networks

Out of the different networks trained, ResNet18 showed the best results. Figure 5 and 6 show the training progress graph. It includes the accuracy and loss percentages.
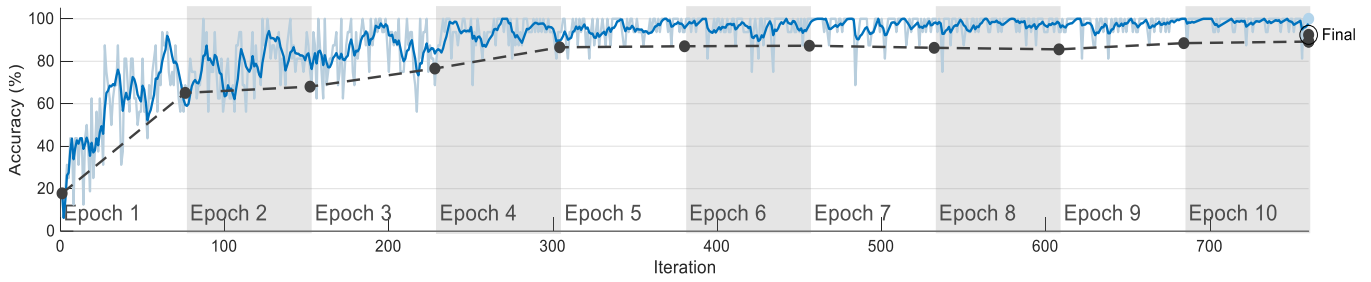
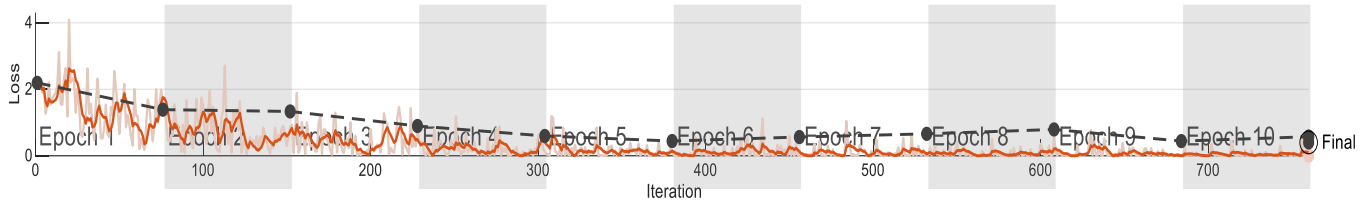Figure 5 Training and Validation accuracy Plot for ResNet18

Figure 6 Training and Validation loss plot for ResNet18

ResNet18 performed the best with 100% training accuracy and 92.43% validation accuracy. The hyperparameters set for this result were the maximum epoch of 10, minimum batch-size of 16 and an initial learn rate of 0.001. This network was exported to the workspace for testing. To understand how well the network has performed on our dataset, confusion matrix is obtained. The diagonal of the matrix represents all the true values and these give the indication of the accuracy of the classification model. The accuracy obtained for the test data set was 93.62%. Following is the confusion chart obtained for the test dataset.
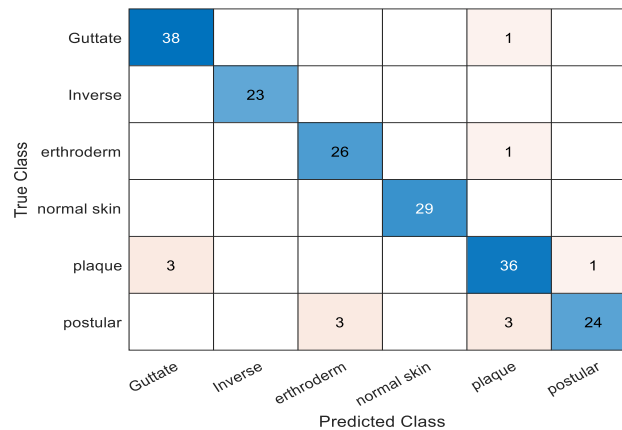
Figure 7 Confusion matrix for test dataset with ResNet18

The performance evaluation parameters were calculated by 3 parameters i.e precision, recall and f1-score. Equations below gives the formulas to depicts these values.

$$precision = \frac{(True\ Positive)}{(True\ Positive) + (False\ Positive)} \tag{1}$$

$$Recall = \frac{(True\ Positive)}{(True\ Positive) + (False\ Negative)} \tag{2}$$

$$F1\ score = 2 * \frac{(Precision) * (Recall)}{(Precision) + (Recall)} \tag{3}$$

Following table 2 shows the evaluation matrix values

Table 2 Performance Evaluation parameters

Class	Accuracy	Precision	Recall	f1-score
Guttate	98.94%	0.97	0.97	0.97
Inverse	98.94%	1	0.92	0.96
Erythrodermic	97.87%	0.89	0.96	0.92
Normal Skin	99.47%	0.97	1	0.98
Plaque	100%	1	1	1
Pustular	97.34%	0.93	0.9	0.92

A good model should have all these values as high as possible in an ideal scenario as it is the measure of how well the model can predict that particular positive class. The values obtained in our case are reasonably good to be considered as a robust model.

V. CONCLUSION

Different networks were employed for the classification of Psoriasis transfer learning and a comprehensive comparison could be achieved between them. Out of the three networks (GoogleNet, Squeezenet, and ResNet18) the best accuracy was shown by ResNet18 with an accuracy of 93.62%. The novelty here is validating the different programming environmental setup, i.e., MATLAB for the classification of medical images. With the best visual data representation and ease of coding, this environment can be a go-to coding platform for non-coders. The results showed the ability to classify the types of Psoriasis accurately, helping doctors to aid to their diagnose and proceed with the treatment accordingly with a more objective addition to the treatment. The accuracy was found to be more than what was achieved by other method done previously. As a future scope, different algorithms such as object detection, K- Nearest Neighbor, K means clustering, and support vector machines can be used to classify Psoriasis.

REFERENCES

[1]   A. B. Kuchekar, R. R. Pujari, S. B. Kuchekar, S. N. Dhole, and P. M. Mule, "Psoriasis: A comprehensive review.," *International Journal of pharmacy & life sciences*, vol. 2, no. 6, 2011.
[2]   A. W. Armstrong, M. D. Mehta, C. W. Schupp, G. C. Gondo, S. J. Bell, and C. E. M. Griffiths, "Psoriasis Prevalence in Adults in the United States," *JAMA Dermatol*, vol. 157, no. 8, pp. 940–946, Aug. 2021, doi: 10.1001/jamadermatol.2021.2007.
[3]   M. Kumar, "AYURVEDIC PERSPECTIVE OF PSORIASIS: A CASE STUDY," 2021.
[4]   A. W. Armstrong and C. Read, "Pathophysiology, clinical presentation, and treatment of psoriasis: a review," *JAMA*, vol. 323, no. 19, pp. 1945–1960, 2020.
[5]   E. M. Farber and L. Nall, "Nail psoriasis.," *Cutis*, vol. 50, no. 3, pp. 174–178, 1992.
[6]   Z. U. Syed and A. Khachemoune, "Inverse psoriasis: case presentation and review," *Am J Clin Dermatol*, vol. 12, pp. 143–146, 2011.
[7]   R. J. G. Chalmers, T. O'sullivan, C. M. Owen, and C. E. M. Griffiths, "A systematic review of treatments for guttate psoriasis," *British Journal of Dermatology*, vol. 145, no. 6, pp. 891–894, 2001.
[8]   R. K. Singh *et al.*, "Erythrodermic psoriasis: pathophysiology and current treatment perspectives," *Psoriasis: Targets and Therapy*, pp. 93–104, 2016.
[9]   E. M. Farber and L. Nall, "Pustular psoriasis.," *Cutis*, vol. 51, no. 1, pp. 29–32, 1993.
[10]   U. Withana and P. Fernando, "Differential diagnosis of eczema and psoriasis using categorical data in image processing," in *2017 Seventeenth International Conference on Advances in ICT for Emerging Regions (ICTer)*, IEEE, 2017, pp. 1–6.
[11]   N. Garzorz-Stark *et al.*, "A novel molecular disease classifier for psoriasis and eczema," *Exp Dermatol*, vol. 25, no. 10, pp. 767–774, 2016.
[12]   S. Kim *et al.*, "Smartphone-based multispectral imaging and machine-learning based analysis for discrimination between seborrheic dermatitis and psoriasis on the scalp," *Biomed Opt Express*, vol. 10, no. 2, pp. 879–891, 2019.
[13]   D. Padilla, A. Yumang, A. L. Diaz, and G. Inlong, "Differentiating atopic dermatitis and psoriasis chronic plaque using convolutional neural network mobilenet architecture," in *2019 IEEE 11th International Conference on Humanoid, Nanotechnology, Information Technology, Communication and Control, Environment, and Management (HNICEM)*, IEEE, 2019, pp. 1–6.
[14]   T. Okamoto, M. Kawai, Y. Ogawa, S. Shimada, and T. Kawamura, "Artificial intelligence for the automated single-shot assessment of psoriasis severity," *Journal of the European Academy of Dermatology and Venereology*, vol. 36, no. 12, pp. 2512–2515, 2022.
[15]   M. J. Schaap, N. J. Cardozo, A. Patel, E. De Jong, B. Van Ginneken, and M. M. B. Seyger, "Image-based automated Psoriasis Area Severity Index scoring by Convolutional Neural Networks," *Journal of the European Academy of Dermatology and Venereology*, vol. 36, no. 1, pp. 68–75, 2022.
[16]   R. G. Langley and C. N. Ellis, "Evaluating psoriasis with psoriasis area and severity index, psoriasis global assessment, and lattice system physician's global assessment," *J Am Acad Dermatol*, vol. 51, no. 4, pp. 563–569, 2004.
[17]   C. Ozgur, T. Colliau, G. Rogers, and Z. Hughes, "MatLab vs. Python vs. R," *Journal of data Science*, vol. 15, no. 3, pp. 355–371, 2017.
[18]   J. G. Carbonell, R. S. Michalski, and T. M. Mitchell, "An overview of machine learning," *Mach Learn*, pp. 3–23, 1983.
[19]   S. M. Anwar, M. Majid, A. Qayyum, M. Awais, M. Alnowami, and M. K. Khan, "Medical image analysis using convolutional neural networks: a review," *J Med Syst*, vol. 42, pp. 1–13, 2018.
[20]   N. Tajbakhsh *et al.*, "Convolutional neural networks for medical image analysis: Full training or fine tuning?," *IEEE Trans Med Imaging*, vol. 35, no. 5, pp. 1299–1312, 2016.
[21]   S. F. Aijaz, S. J. Khan, F. Azim, C. S. Shakeel, and U. Hassan, "Deep learning application for effective classification of different types of psoriasis," *J Healthc Eng*, vol. 2022, 2022.
[22]   N. Amin and M. S. Farooq, "Automated Psoriasis Detection using Deep Learning," 2021.
[23]   V. K. Shrivastava, N. D. Londhe, R. S. Sonawane, and J. S. Suri, "Reliable and accurate psoriasis disease classification in dermatology images using comprehensive feature space in machine learning paradigm," *Expert Syst Appl*, vol. 42, no. 15–16, pp. 6184–6195, 2015.
[24]   M. Dash, N. D. Londhe, S. Ghosh, A. Semwal, and R. S. Sonawane, "PsLSNet: Automated psoriasis skin lesion segmentation using modified U-Net-based fully convolutional network," *Biomed Signal Process Control*, vol. 52, pp. 226–237, 2019.
[25]   L.-H. Juang and M.-N. Wu, "Psoriasis image identification using k-means clustering with morphological processing," *Measurement*, vol. 44, no. 5, pp. 895–905, 2011, doi: https://doi.org/10.1016/j.measurement.2011.02.006.
[26]   K. Yu, M. N. Syed, E. Bernardis, and J. M. Gelfand, "Machine learning applications in the evaluation and management of psoriasis: a systematic review," *J Psoriasis Psoriatic Arthritis*, vol. 5, no. 4, pp. 147–159, 2020.
[27]   C. Navarrete-Dechent, S. W. Dusza, K. Liopyris, A. A. Marghoob, A. C. Halpern, and M. A. Marchetti, "Automated dermatological diagnosis: hype or reality?," *J Invest Dermatol*, vol. 138, no. 10, p. 2277, 2018.
[28]   A. Abraham, K. Sobhanakumari, and A. Mohan, "Artificial intelligence in dermatology," *Journal of Skin and Sexually Transmitted Diseases*, vol. 3, no. 1, pp. 99–102, 2021.

Characterisation of low-frequency artifacts and their removal in magnetocardiograms

S. Sengottuvel
SQUIDs Applications Section
SQUID & Detector Technology
Division, Materials Science Group,
Indira Gandhi Centre for Atomic
Research, Kalpakkam-603 102
sengo@igcar.gov.in

S. Shenbaga Devi
Centre for Medical Electronics,
Department of Electronics &
Communication Engineering,
College of Engineering Guindy,
Anna University, Chennai-600 025
s_s_devi@annauniv.edu

M. Sasikala
Centre for Medical Electronics,
Department of Electronics &
Communication Engineering,
College of Engineering Guindy,
Anna University, Chennai-600 025
sasikala@annauniv.edu

Abstract— **Non-invasive and non-contact measurement of subtle magnetic fields generated by the electrical activity of the heart is magnetocardiography (MCG) and is known to offer distinct diagnostic information than ECG. Superconducting quantum interference device (SQUID) sensors that have unparalleled sensitivity is used to measure MCG inside a magnetically shielded room by attenuating extraneous electromagnetic interferences. However, biological artifacts imposed by subjects pose a challenging situation in quantifying the inherent low-frequency diagnostic information present in MCG which is severely corrupted by drifts. This work discuses a methodical approach to rightly identify and discriminate low-frequency artifacts arising from gastric sources and respiratory movements of subjects which ride over low-frequency cardiac signals present in a multichannel MCG data. The work details exclusive evaluations performed to confirm the origins of these artifacts and utilizing them to assess the adequacies of filtering methods for the optimal removal of low-frequency drift components from MCG.**

Keywords— MCG, SQUID sensors, breathing artifacts, gastric artifacts

I. INTRODUCTION

Magnetocardiography (MCG) is the measurement of extremely weak magnetic fields emanating from the electrical activity of the heart [1]. These signals are of the order of 1 – 100 pico Tesla (pT) and could be measured by highly sensitive superconducting quantum interference device (SQUID) sensor inside magnetically shielded room. These shielded rooms attenuate background electromagnetic fields and a noise floor of ~ 12 femto Tesla (fT) is facilitated to record biomagnetic fields. SQUID sensors are immersed in liquid Helium filled inside plastic cryostats and the subjects at room temperature are positioned supinely with chest closer to the tail of the cryostat. MCG measured using multichannel SQUID array offers comprehensive diagnostic information which is complementary to ECG [1]. However, SQUID is also sensitive to other interferences in the vicinity of the MCG system inside the shielded room including the biological artifacts from subjects themselves from whom MCG is measured. Low-frequency artifacts from subjects imposed on MCG are usually seen as drifts riding over cardiac signals. While interferences whose frequency characteristics are known apriori could be eliminated by suitable filters, noise occurring at lower frequencies (< 2 Hz) is difficult to distinguish from the useful diagnostic information present in this frequency regime such as the near-DC level variations of the cardiac cycle in the ST-T region of the cardiac cycle. The low-frequency cardiac signals are useful in the diagnosis of the electrical signals associated with reduced supply of blood to the heart, the ischemic heart diseases [2]. It is generally believed that the relative movement of the chest wall of subjects about the sensor array causes breathing artifacts [3]. However, no exclusive study is found in the literature to comprehensively study the range of drift variations, their spatial distribution, anatomical origin, and the degree of influence on the MCG time series. It is expected that such a characterization would better define the requirements for artifact correction methods applied to MCG signals, such that the inherent low-frequency cardiac signals are unaffected.

II. METHODS, ANALYSIS & DISCUSSION

A. Experimental

MCG was measured for a set of subjects by positioning them under the cryostat in supine rest conditions. The present measurement consisted of recording MCG over the whole torso of subjects and analyzing the as-measured raw MCG which contained cardiac time series and the low-frequency drifts which ride over the PQRST waveforms. These two apparently different signal and noise components were individually inspected to confirm their origins for further analysis.

B. Analysis-Respiration

The low-frequency drift components in the MCG system used in the present work [3] were verified for their possible association with respiration by simultaneously recording two independent respiratory sensors namely a thermistor which records local variations in temperature of exhaled air near nostril and an accelerometer fixed on the waist of subjects to measure changes

in body movements due to respiration. The similitude of variations occurring in both the sensors was compared against the envelope of an MCG channel corrupted by the drift. Figure 1 illustrates this experiment on a subject whose frequency of breathing happened at a lower frequency of 0.04 Hz (respiratory rate of 2.4 cycles per minute (cpm)) which eventually affirmed the association between the drift artifact and respiration [4].
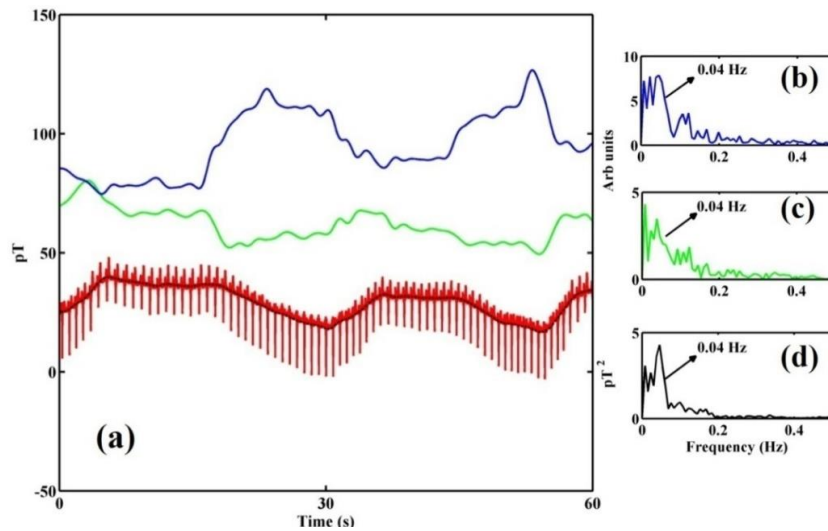

Fig. 1. Simultaneous measurement of MCG and respiratory sensors (a) As-measured MCG (red trace) riding over low-frequency drift (black envelope). Estimates of respiration measured by thermistor (blue trace) and by accelerometer (green trace). (b)-(d) Fast Fourier transform (FFT) of signals in (a) indicating breathing peaks at 0.04 Hz (2.4 cpm)

C. Analysis-Dipolar nature of spatial distribution of signal components

The bio-magnetic fields measured on the body surface are known to exhibit dipolar patterns with positive and negative variations of the flux lines around current dipole sources which are reported to be not observed for that of the artifacts [1]. Figure 2 features the spatio-temporal contour maps of drift components recorded over 60 locations on the torso of a subject exhibiting non-dipolar nature of drift components and their magnitude levels (colour range in the contours) were found to be far exceeding that seen for the PR and ST segments (shown here as an example) with clear dipolar variations as expected for signal components [1] [3]. Figure 3 shows a similar behaviour of the contours generated at the time instant of drifts in a different sensor array and they were seen to be dominant especially in the inferior channels of the MCG scanning area. As seen in the figure, the spectral powers of drifts revealed two distinct low frequencies, 0.05 Hz (3 cpm) and 0.3 Hz (18 cpm). Further, the 3 cpm low-frequency peaks were seen to be dominant near gastric area and were conspicuously absent in the far-away channels as indicated.
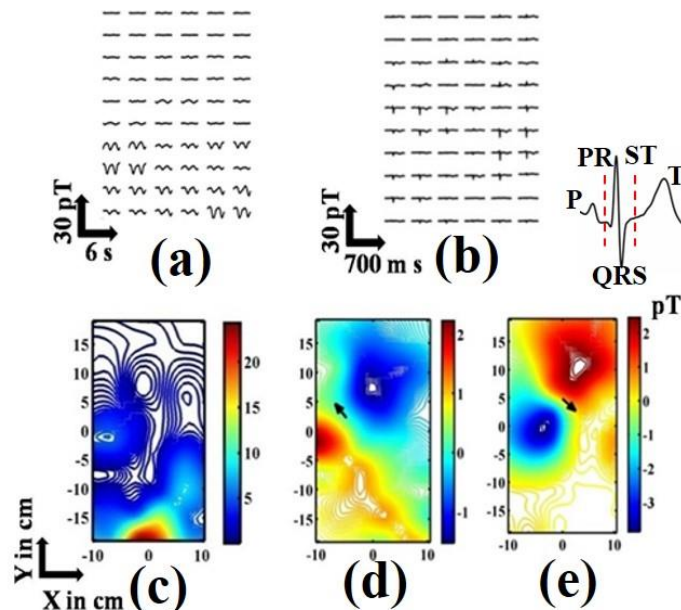

Fig. 2. Spatial distribution of magnetic fields on the torso of a subject for (a) low-frequency drift (b) MCG traces of one cardiac cycle (c) spatio-temporal contour map at a time instant of the drift, (d) and (e) contour maps showing dipolar features at PR and ST segments. Arrows in the contour signify the current dipoles which generate the magnetic field distributions
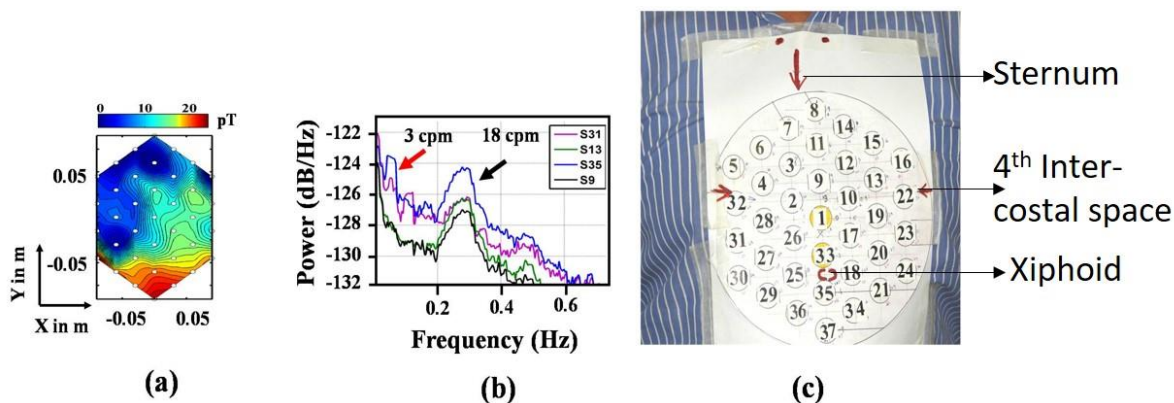
Fig. 3. Identification of other low-frequency components in MCG (a) Spatio-temporal map of drift components showing higher magnitudes in the inferior channels (b) FFT of a few MCG channels showing two distinct low-frequencies 3 and 18 cpm at inferior locations (c) MCG measurement grid pasted on the chest

Hence, this observation persuaded looking in to the origin of these drifts at inferior channel locations of MCG. Further, in order to confirm that 3 cpm spectral peaks were not due to the non-stationary respiratory patterns (slow and normal breathing cycles); measurements were exclusively focused on the upper abdomen, over the stomach of subjects and the drifts were measured before and three hours after food for subjects.

D. Analysis-Gastric signal components

Figure 4 shows the characteristic variations in low-frequency drifts before-and-after food which unequivocally validate that the drifts at inferior channel locations of MCG are gastric slow-waves (3 cpm). Magnetic fields generated by gastric electrical activity are well reported by researchers [5]. The overall increase in the power spectral density (PSD) of these drifts in the abdomen of all the measurement channels for four subjects are tabulated in Table 1, represented as mean +/- standard deviation. It was found that for three out of four subjects, the post-prandial increase in low-frequency power was significant. Hence the dominance of low-frequency artifacts in MCG measurements was hence confirmed in part contributed by gastric signals in the inferior channel locations of routine MCG position.
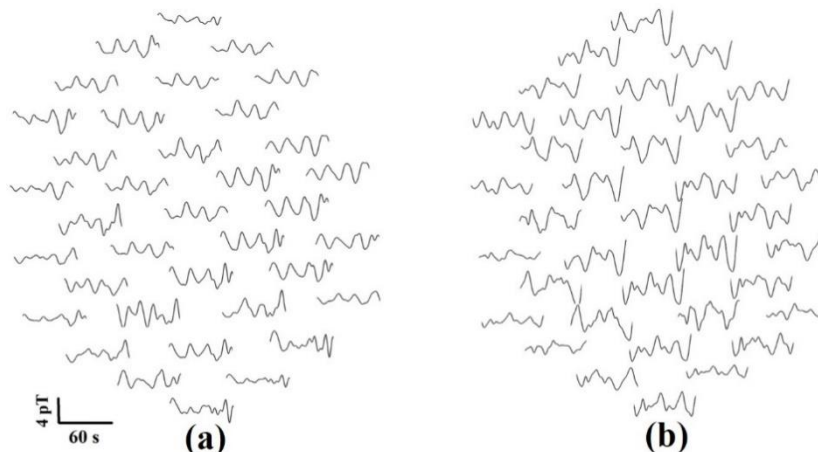

Fig. 4. Spatial distribution of low-frequency drifts of a subject (a) before and (b) after-food

TABLE 1 PRE-AND-POST-PRANDIAL POWER OF DRIFTS IN ABDOMEN

	PSD (dB/Hz)	
Subject	Pre-prandial	Post-prandial
Sub#1	-138 ± 9	-136 ± 3
Sub#2	-125 ± 10	-121 ± 13
Sub#3	-118 ± 15	-116 ± 7
Sub#4	-132 ± 18	-135 ± 23

III. SIMULATION OF LOW-FREQUENCY DRIFTS AND EVALUATION OF DRIFT CORRECTION METHODS

These inferences were utilized to test the performance of some conventional drift correction methods viz, cubic-spline interpolation (CSI), empirical mode decomposition (EMD) and wavelet (WAV) filtering. In order to create measurement conditions involving different combinations of low-frequency drifts which are sufficiently capable of influencing MCG, an actual MCG time series was added with varying magnitudes of simulated drifts and tested with the drift correction methods to assess their efficiency as shown in Figure 5.
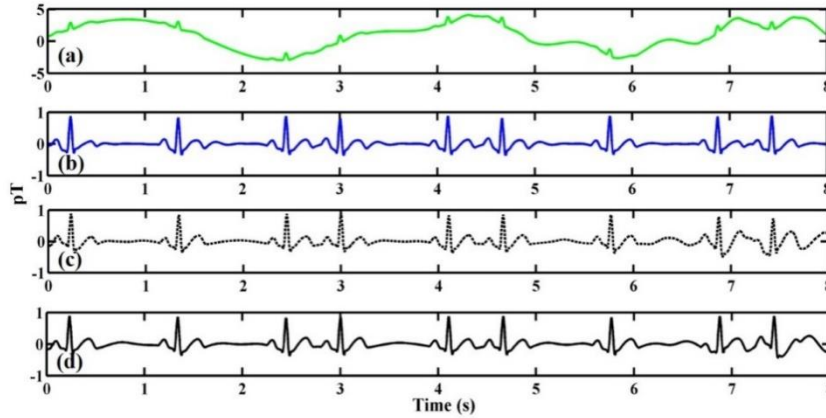

Fig. 5. Comparison of drift correction methods in eliminating low-frequency artifacts in MCG (a) Raw MCG corrupted by gastric and breathing drift which is corrected by (b) cubic-spline method (c) EMD filter (d) wavelet filter

Table 2 tabulates the maximum value of error (in pico and femto Tesla) measured in the ST segment of the MCG time series corrupted by different combinations of low-frequency drifts and that corrected by the three different conventional methods [2]. In order to incorporate the non-stationary behavior of the drifts, chirp signal with continuously varying frequencies from 0.05-0.3 Hz was also added to MCG. It was found that CSI outperformed other methods in efficiently removing drifts as noticed from the least distortion in the ST segment, i.e. inherent low-frequency signal component. The superiority of CSI is attributed to the fact drift estimation is independent of frequency unlike EMD and WAV which act as tunable filters to appropriately select a frequency band containing unwanted low-frequency drift artifact to be eliminated from the raw time series [3]. Hence a mixing of different drift frequencies (gastric, respiratory components and their dynamics) challenges proper identification and elimination of artifacts in EMD and WAV.

TABLE 2 PERFORMANCE OF DRIFT CORRECTION METHODS FOR DIFFERENT COMBINATIONS OF DRIFTS IN MCG

Sl. No	Y1 Chirp	Y2 Gast	Y3 Resp	Max error in ST segment (fT)		
	Magnitude (pT)			CSI	WAV	EMD
1	-	12	-	200	360	360
2	-	-	80	220	4000	8000
3	-	6	28	100	2000	3000
4	-	15	100	200	6000	12000
6	-	60	-	120	500	1000
7	20	2	2	3000	4800	7000

IV. CONCLUSION

The involvement of respiratory drifts on cardiac signals in general and MCG in particular is known in the literature, however, an important contribution of this study is the identification of the role of gastric artifact in addition to the respiratory contributions which corrupt MCG. More importantly, the present study outlines a methodical approach of tracking these artifacts in a controlled environment unequivocally with the help of simultaneously recorded MCG signals across different locations over the chest. The present study thus particularly emphasizes due attention to be paid on multichannel MCG especially on the inferior channel locations for their possible influence by gastric signals (especially post-prandial slow wave drifts). Secondly, irrespective of the nature and origin of drifts in MCG, as highlighted in the simulation study, the use of frequency-independent drift correction methods like cubic-spline techniques will be beneficial in safeguarding inherent low-frequency cardiac information like the PR and ST segments which are important in several cardiac investigations where MCG is already known for its technological advantage as opposed to the conventional ECG [1].

REFERENCES

[1] J. Clarke and Braginski A. I. (ed) 2006, The SQUID Handbook: Applications of SQUIDS and SQUID Systems vol 2, First Edition (Weinheim: Wiley-VCH).

[2] S. Lenis, N. Pilia, A. Loewe and W.H.W. Schulze , "Comparison of Baseline Wander removal Techniques considering the Preservation of ST Changes in the Ischemic ECG: A Simulation Study", Comp & Math Method in Med., 2017, 1-13.

[3] N. Mariyappa, S. Sengottuvel, R. Patel, C. Parasakthi et al., "Denoising of multichannel MCG data by the combination of EEMD and ICA and its effect on the pseudo current density maps", Biomed Sigproc & Cntrl., 2015, 18, 204-13.

[4] S. A. Shea, " Behavioural and arousal-related influences on breathing in humans", Exp Physiol., 1996, 81(1), 1-26.

[5] S. Somarajan, N. D. Muszynski, D. Hawrami, J. D. Olson, L. K. Cheng and L. A. Bradshaw, "Noninvasive magnetogastrography detects erythromycin-induced effects on gastric slow wave ", IEEE Trans BME., 2018, 66(2), 327-334.

A FRAMEWORK FOR IDENTIFICATION OF RESPIRATORY DISEASES USING GENERATIVE ADVERSARIAL NETWORK ANDMULTICLASS MODELS

Varoon K
Department of Electronics Engineering
Madras institute of technology Chennai, India
varoonsandeep25@gmail.com

Naveenkumar S
Department of Electronics Engineering
Madras institute of technology Chennai, India
naveensk.offical@gmail.com

Dhanesh K
Department of Electronics Engineering
Madras institute of technology Chennai, India
dhaneshkamaraju@gmail.com

Dr.Kavitha G
Department of Electronics Engineering
Madras institute of technology Chennai, India
kavithagmit@gmail.com

Abstract

CXR imaging is a valuable tool used to diagnose various medical conditions, especially respiratory diseases, which are prevalent due to environmental and genetic factors. Lung diseases are a significant risk, particularly in low-income countrieswhere poverty and harmful pollutants are prevalent. Fortunately, new diagnostic technologies like X-ray machines offer low-cost and convenient test options, emitting lower levels of radiation than CT scans.

Recent developments in medical imaging include the use of deep learning techniques like Convolutional Neural Networks (CNN) and Support Vector Machines (SVMs) to analyze radiological images. SVMs can classify lung diseases into four categories:Covid-19, Pneumonia, Tuberculosis, and healthy, which can help improve the accuracy of diagnoses and treatment.

To enhance diagnostic accuracy, it is crucial to adopt efficient diagnostic systems like Generative Adversarial Networks (GAN),which create synthetic images that can be used to improve SVM's performance for multi-classification of five categories. Analyzingthe SVM model's results using ROC curves helps determine sensitivity and specificity, enabling informed decision-making by healthcare providers.

Overall, these advances in medical imaging hold great promise for improving public health outcomes, especially in diagnosing and managing respiratory diseases.

Index Terms

Generative Adversarial Networks, Support Vector Machines, CXR images

I. INTRODUCTION

The lungs are a vital component of the respiratory system, which enables the exchange of oxygen and carbon dioxide between the body and the environment. Unfortunately, lung diseases can disrupt this delicate balance, leading to various medical conditions that can affect the quality of life and even result in mortality. Lung disorders can be caused by a range of factors, including infections, pollutants, genetic factors, and lifestyle choices. Therefore, the accurate diagnosis and classificationof lung diseases are crucial for effective treatment and management.

Medical imaging techniques, such as X-rays, CT scans, and MRI, provide clinicians with a non-invasive and cost-effectiveway to visualize the lungs and identify any abnormalities or pathologies. Among these techniques, X-ray imaging is particularlyuseful for diagnosing and monitoring lung diseases due to its widespread availability and low cost. However, the interpretation of X-ray images requires expertise and experience, and misinterpretations can lead to incorrect diagnoses or delayed treatment.To assist in the interpretation of X-ray images, machine learning algorithms such as Support Vector Machines (SVM) can be trained to classify lung diseases based on the visual features present in the images. SVM is a supervised learning model thatuses a technique called the kernel trick to transform data and determine an optimal boundary between the different classes. There are two types of SVM: simple or linear SVM and kernel or non-linear SVM, and the choice depends on the complexityof the problem at hand.

However, one common problem with medical imaging datasets is the imbalance of the number of samples in each class, which can lead to bias and misclassification. To address this issue, Generative Adversarial Networks (GANs) can be used to generate synthetic images that can be added to the dataset to balance the number of samples. GANs are a type of deep learning model that uses a generator and a discriminator to create new data that resembles the real data. GANs have been shown to be effective in generating synthetic medical images that can be used to augment the training dataset and improve the performance of machine learning algorithms.

In this work, we propose a method that combines GAN-generated synthetic images with SVM classification to diagnose and classify lung diseases. The GAN-generated images are preprocessed and normalized to ensure they are consistent with the real images, and then used to augment the training dataset for SVM. The performance of the SVM model is evaluated using metrics such as sensitivity, specificity, and ROC curves, and compared to SVM without GAN-generated data. Our results show that the combination of GAN and SVM can improve the accuracy of lung disease classification, especially for underrepresented classes such as tuberculosis. By providing a more accurate and efficient way to diagnose and classify lung diseases, this method hasthe potential to improve patient outcomes and reduce healthcare costs.

II. METHODOLOGY

A. GAN Architecture

Generative Adversarial Network (GAN) is a deep learning model that comprises of two neural networks, the generator andthe discriminator, that compete against each other in a zero-sum game framework. The goal of GANs is to generate new,synthetic data that resembles a known data distribution. The generator component of the GAN model produces synthetic datasamples by decoding or upsampling a random vector of noise from the Z-space using a transpose convolutional technique.This process results in an image of the original dimension. The generator learns to create fake data by incorporating feedbackfrom the discriminator and adjusting its output to make it appear real. The discriminator, on the other hand, acts as a classifierand attempts to distinguish between real data instances and fake data instances generated by the generator. The discriminatorreceives training data from two sources, real data instances and fake data instances generated by the generator. Real datainstances serve as positive examples, while fake data instances serve as negative examples during the discriminator's training.During the training process, the generator and the discriminator play a zero-sum game, where the generator aims to produce synthetic data samples that are similar to the real data distribution, while the discriminator aims to correctly classify the real data and identify the fake data generated by the generator.
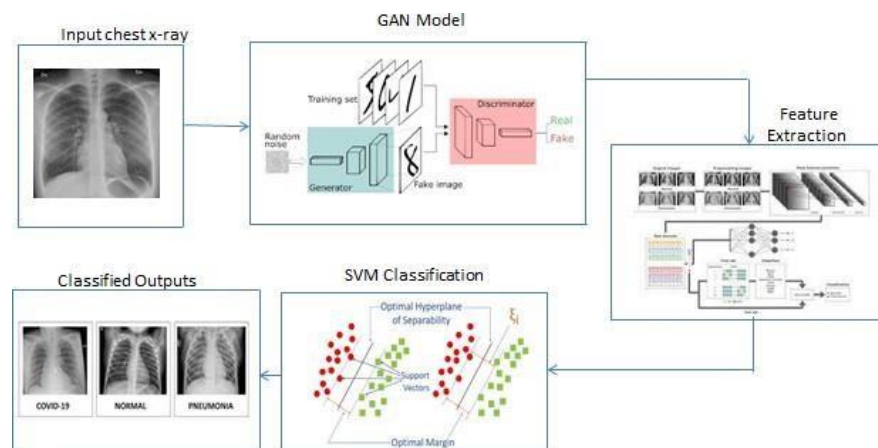

Fig. 1: Technical Architecture

B. Dataset

The CXR images were obtained from the Kaggle forum provided by University of Doha, Qatar. The acquired dataset is composed of 5 classes. The sample count of covid-19 are 3600. The sample count of viral pneumonia are 2000. The sample count of bacterial pneumonia are 1700. The sample count of tuberculosis are 500. The samples count of normal lung are 3000.

The images have some unwanted noise and medical details. The images were need to be preprocessed. All the images are resized to 256 X 256 dimensions.

C. Classification

Image classification is an supervised learning algorithm used to classify an image based on the classes. Features are extracted,normalized, standardized before feeding into a machine learning model for classification task. The classifier learns the featureof a class and thereby separating the images. There are many machine learning classifiers that handles the image classification such as Decision trees, Logistic Regression, Support Vector machines.But SVM is the preferable choice since SVM classifier predominantly works well for featured data and for binary classification. The features extracted from images are then normalizedand feed to the SVM model for multiclass classification. The binary classification were done between normal and others .The classification using SVM performed on normal Vs abnormal, normal Vs tuberculosis, normal Vs bacterial pneumonia, normal Vs covid-19, normal Vs viral pneumonia.

III. EXPERIMENTAL RESULTS

From the Table 1, the test accuracy of normal Vs abnormal and normal Vs tuberculosis is significantly increases when using images generated out of GAN. For every 50 epochs of training the GAN, GAN generates the chest X-ray image of tuberculosis accurately. After 500 epochs of training, GAN model delivers tuberculosis images which has the highest accuracy for the SVM model trained later.

We evaluated our proposed GAN model on a dataset of CXR images and compared its performance with several state-of-the-artmodels. The dataset contained over 10000 CXR images of varying sizes and resolutions. We also performed a qualitative evaluation by comparing the generated images with the ground truth images using visual inspection. The results of our experiments demonstrate that the proposed GAN model outperformed the state-of-the-art models in terms of both quantitative and qualitative evaluation metrics.

Moreover, the generated CXR images by our proposed GAN model showed better details, better contrast, and better image quality compared to the state-of-the-art models. The visual inspection showed that the generated images had sharper edges, clearer organs, and better texture details. To further validate the effectiveness of our proposed GAN model, we conducted a userstudy.

The results of the user study demonstrated that our proposed GAN model generated more realistic CXR images compared to thestate-of-the-art models. The users also reported that the generated images by our GAN model had better diagnostic value and were more useful for medical professionals. Overall, our experimental results demonstrate that the proposed GAN model is highly effective for generating high-quality CXR images, which can be useful for medical professionals in diagnosis and treatment planning.

We compared our GAN model with several state-of-the-art image generation models and found that it outperformed them in terms of all three evaluation metrics. Specifically, our GAN model had a higher IS score, lower FID score, and higher PSNR score compared to the other models. These results suggest that our GAN model is highly effective for generating CXR images that are both visually appealing and highly similar to the input data. This could have important applications in medical imaging, where high-quality image generation can be useful for training machine learning models and aiding in diagnosis and treatment planning.We also performed a visual inspection of the generated images and found that they exhibited clear anatomical structures and well-defined features, such as lung fields and diaphragms. Moreover, the generated images showed good contrast and sharpness, with no obvious artifacts or distortions.

Overall, our experimental results demonstrate that our GAN model is highly effective for generating high-quality CXR images that are both visually appealing and useful for medical professionals in diagnosis and treatment planning. The model has important applications in medical imaging, where it could be used to generate synthetic data for training machine learning models or to aid in the interpretation of medical images.

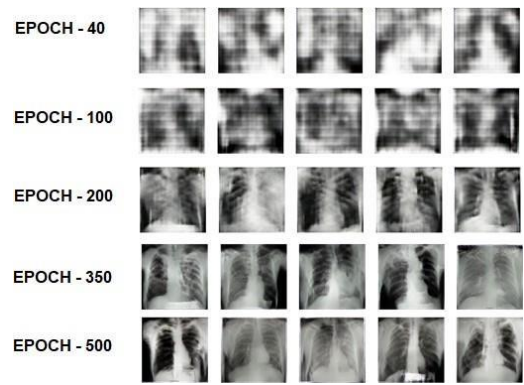| Performance measures		Without GAN	With GAN
Normal Vs Abnormal	Training accuracy	0.985	0.978
	Test accuracy	0.806	0.881
Normal Vs Tuberculosis	Training accuracy	0.875	0.893
	Test accuracy	0.858	0.881

Table1. Performance measures for binary classification

Fig2. Synthetic X-ray images of Tuberculosis generated using GAN

Figure 3 and Figure 4 shows the Regional Operating Characteristics plot for the normal Vs abnormal classification and normal Vs tuberculosis classification using Support Vector Machines.
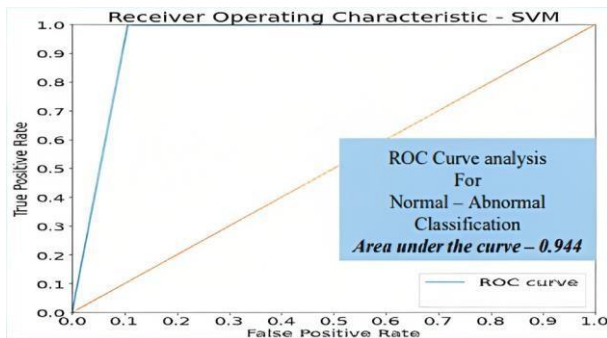

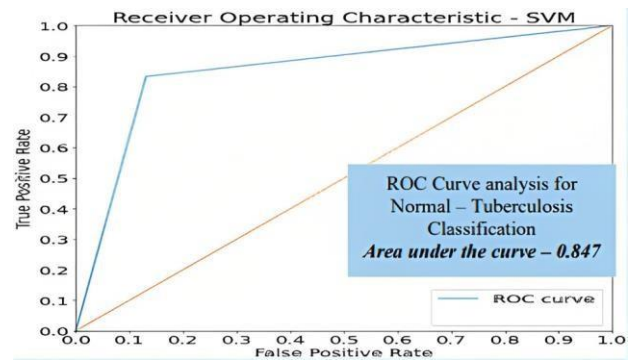Fig3. ROC curve for Normal Vs Abnormal classification classification

Fig4. ROC curve for Normal Vs Tuberculosis

IV. CONCLUSION

Without the augmentation process using GAN, the number of samples used for tuberculosis is 500. With augmentation using GAN, 300 more tuberculosis samples are generated. The latent dimension and epoch used for entire GAN modeling is 200 and 500 respectively. The binary classification of normal-abnormal has been done using SVM classifier. The testing accuracy are found to be 0.881 when GAN used and 0.806 when GAN is not used. Then the binary classification of normal Vs each class has been done using SVM classifier. The testing accuracy is found to be 0.936 for normal Vs bacterial pneumonia classification. The testing accuracy is found to be 0.945 for normal Vs viral pneumonia classification. The testing accuracy is found to be 0.951 for normal Vs covid classification. The testing accuracy is found to be 0.881 when GAN used and 0.858 when GAN is not used for normal Vs tuberculosis classification. Therefore, SVM classifier performs better when trained on more data generated out of GAN. In this work, multiclass classification from CXR images has been carried out by machine learning models such as Support Vector Machines and Generative Adversarial Networks. The chest X-ray images were obtained from the kaggle forum provided by University of Doha, Qatar and 5000 images were used for training pro- cess. Before training, preprocessing is done to improve quality and remove unnecessary channels in images. To alleviate data mismatch problem of tuberculosis class, image augmentation using GAN is done to artificially create synthetic images to expand dataset size. Without the augmentation process using GAN, the number of samples used for tuberculosis is 500. With augmentation using GAN, 300 more tuberculosis samples are generated. The latent dimension and epoch used for entire GAN modeling is 200 and 500 respectively. The binary classification of normal-abnormal has been done using SVM classifier. The testing accuracy are found to be 0.881 when GAN used and 0.806 when GAN is not used. Then the binary classification of normal Vs each class has been done using SVM classifier. The testing accuracy is found to be 0.936 for normal Vs bacterial pneumonia classification. The testing accuracy is found to be 0.945 for normal Vs viral pneumonia classification. The testing accuracy is found to be 0.951 for normal Vs covid classification. The testing accuracy is found to be 0.881 when GAN used and 0.858 when GAN is not used for normal Vs tuberculosis classification. Therefore, SVM classifier performs better when trained on more data generated out of GAN.

REFERENCES

[1] Rajaraman S, Candemir S, Kim I, Thoma G, Antani S, *Visualization and interpretation of convolutional neural network predictions in detecting pneumonia in pediatric chest radiographs*, Lister Hill National Center for Biomedical Communications, National Library of Medicine, Bethesda, MD 20894, USA Appl. Sci. 2018, 8(10), 1715.

[2] Y. Wei, S. Xu, S. Tran and B. Kang, *Data Augmentation with Generative Adversarial Networks for Grocery Product Image Recognition*, 16th International Conference on Control, Automation, Robotics and Vision (ICARCV), 2020.

[3] Waheed, A., Goyal, M., Gupta, D., Khanna, A., Al-Turjman, F., Pinheiro, P.R., *Covid GAN: data augmentation using auxiliary classifier GAN for improved COVID-19 detection*, IEEE Access 8, 91916–91923 (2020).

[4] D. Uke, K. K. Soni and A. Rasool, *Support Vector Machine for Multiclass Classification*, 11th International Conference on Computing, Communication and Networking Technologies (ICCCNT), pp. 1-6,2020.

[5] Jain G, Mittal D, Thakur D, Mittal M, *A deep learning approach to detect Covid-19 coronavirus with X-ray images*, Biocybern Biomed Eng, October-December; 40(4): 1391–1405d, 2020.

[6] Jagriti Kalyani and Monisha Chakraborty, *Contrast Enhancement of X-ray Images using Histogram Equalization Techniques*, International Conference on Computer, Electrical and Communication Engineering,vol 2, pp.20-23,2020.

[7] Omprakash Patel, Yogendra P. S. Maravi and Sanjeev Sharma, *A Comparative Study of Histogram Equalization based Image Enhancement Techniques for Brightness Preservation and Contrast Enhancement*, Signal Image Processing : An International Journal, vol.3, pp.11-23,2013.

[8] Sayanti Mukherjee, Lance Rintamaki, Janet L. Shucard, Zhiyuan Wei, Lindsey E. Carlasare, Christine A. Sinsky, *A Statistical Learning Approach to Evaluate Factors Associated With Post-Traumatic Stress Symptoms in Physicians: Insights From the COVID-19 Pandemic*, IEEE Access, vol.10, pp.114434-114454, 2022.

[9] T. Ozturk, M. Talo, E. A. Yildirim, U. B. Baloglu, O. Yildirim, and U. R. Acharya, *Automated detection of COVID-19 cases using deep neural networks with X-ray images*, Comput. Biol. Med, vol.121, pp.103792, Jun. 2020.

[10] U. K. Lopes and J. F. Valiati, *Pre-trained convolutional neural networks as feature extractors for tuberculosis detection*, Comput. Biol. Med., vol. 89, pp. 135–143, Oct. 2017.

Design of Microphone based Smart Stethoscope using Wio Terminal

S. Hema Priyadarshini
Department Of Medical Electronics Engineering
Dayananda Sagar College Of Engineering
Bangalore, India
priyadhema@gmail.com

Aishwarya Prabhu
Department Of Medical Electronics Engineering
Dayananda Sagar College Of Engineering
Bangalore, India
aishwaryaprabhu39.ap@gmail.com

Sahana P
Department Of Medical Electronics Engineering
Dayananda Sagar College Of Engineering
Bangalore, India
sahanap122000@gmail.com

Saritha Pal
Department Of Medical Electronics Engineering
Dayananda Sagar College Of Engineering
Bangalore, India
sarithapaldsml@gmail.com

Surabhi A S
Department Of Medical Electronics Engineering
Dayananda Sagar College Of Engineering
Bangalore, India
surabhias23@gmail.com

Abstract - **A stethoscope is a clinical gadget intended for the procedure of paying attention to inward sounds emerging inside organs of a human or creature body otherwise called auscultation. An electronic stethoscope is utilized to record, break down and enhance the heart and respiratory hints of a human. Two major advances specifically signal conditioning and signal processing are utilized to plan a stethoscope framework. This exposition presents a plan which is a computerized framework implanted in a customary acoustic stethoscope to channel and deal with a sign. There are mainly three components used of which, one comprises of a stethoscope, other one with MAX4466 microphone with amplifier and Wio terminal. The goal is pointed toward dissecting lung sounds. Results obtained from the trials will exhibit expulsion of commotion and sound enhancements which helps the practitioner in better understanding of the internal organs.**

Keywords— Lung sounds, Microphone, Stethoscope, Wio terminal.

I. Introduction

More children die from lung diseases and acute lower respiratory infections than from HIV and malaria combined each year, killing about 1 million [1]. The stethoscope is a well-known medical instrument used to get a preliminary reading on the heart rate of a patient. In the past, stethoscopes were designed so that the patient and the doctor had to be in close proximity and make direct physical contact in order to do auscultation [2].

The simplest diagnostic technique for pulmonary dysfunction is auscultation. Acoustic stethoscopes operate by sending sound from a chest piece to the listener's ear through a hollow tube filled with air. The chest piece typically has a bell (hollow shell) and a diaphragm (plastic disc) on each of its two sides. Body sound causes the diaphragm to vibrate when it is placed on the patient, producing sound pressure waves that pass through the tube and are heard by the listener.

An electronic stethoscope (or Steth phone) amplifies body sounds electronically thus overcoming low sound levels in the body [9]. The stethoscope detects artifacts and component cut-offs (frequency response thresholds of electronic stethoscope microphones, pre-amps, amps, and speakers), which by enhancing mid-range sounds while attenuating both high and low-frequency range noises, limits the overall usefulness of the electronically amplified stethoscope.

Electronic stethoscopes are now made available by many companies with the latest technologies. Electronic stethoscopes convert, process, and amplify electrical signals from acoustic sounds for optimal listening [9].

Though lung sounds are easily audible with a stethoscope, the regular heartbeat creates an invasive, quasi-periodic interference that affects how lung sounds are interpreted during clinical auscultations [10].

This system makes use of a stethoscope, a MAX 4466 microphone with an amplifier, and a Wio Terminal as its three primary parts. The Wio terminal receives the amplified sound from the stethoscope, classifies it, and displays the results of the classification. The necessity of developing an electronic stethoscope is that the acoustic sounds can be converted into electronic impulses that can then be amplified for enhanced monitoring. Further processing is also possible for these electronic signals which can help in classification.

II. LITERATURE SURVEY

As seen in Fig 1, The Bluetooth low-energy (BLE) technology is used by the prototype system's two wireless communication subsystems. The heart sounds signal was initially received by the acoustic sensor and supplied to the analog-font-end (AFE), where it was pre-amplified and filtered. The signal is then transformed using the ADC in the RFduino microcontroller and delivered wirelessly into a personal computer (PC) where it will be analysed and classified using MATLAB[5]. The smart stethoscope's size, visual appeal, and inclusion of HS on board with an integrated decision-making unit, are requirements for this study.
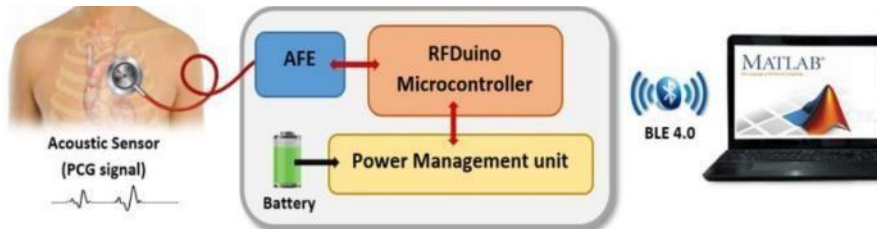
Fig 1. Block diagram real-time smart digital smart stethoscope [5]

As shown in the flow chart of Fig 2, the data acquisition module, the pre-processing module, and the signal processing module are the 3 basic modules of the computer-based cardiac dysfunction detection system using an electronic stethoscope. An electronic stethoscope is used to record the HS for the data collection module, after which it is sent to the pre-processing module after being transformed into digital signals by the related electronics. In the pre-processing module, normalization and segmentation are performed on the filtered and interference-reduced HS signal. Classification and features extraction are under the control of the signal processing module. The system's output is the classification outcome for clinical diagnostic decision-making [10].
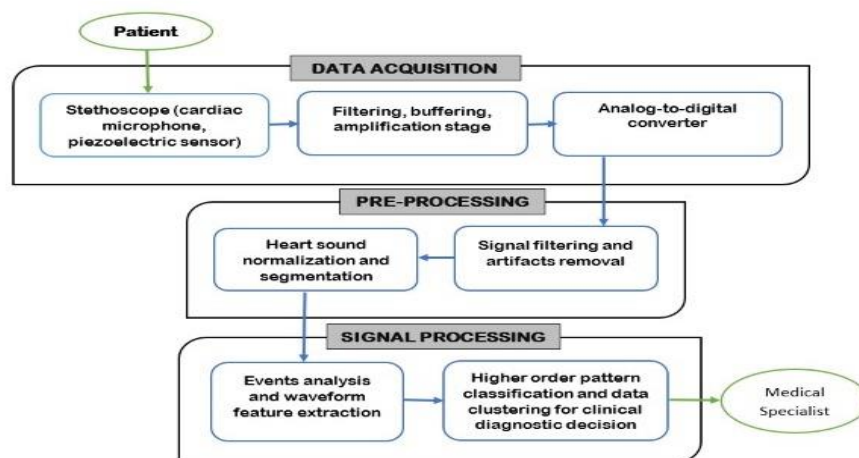

Fig 2. Typical pipeline diagram for signal processing and analysis for heart sounds [10]

III.   METHODOLOGY

The project is built with components that are both affordable and useful. We desire a microcontroller that is both power-efficient and capable of handling inference and audio at the edge. Additionally, the board should be able to show the display on LCD, store audio fileson microSD, and include a few push buttons for navigation. The block diagram of the system is shown in Fig 3.
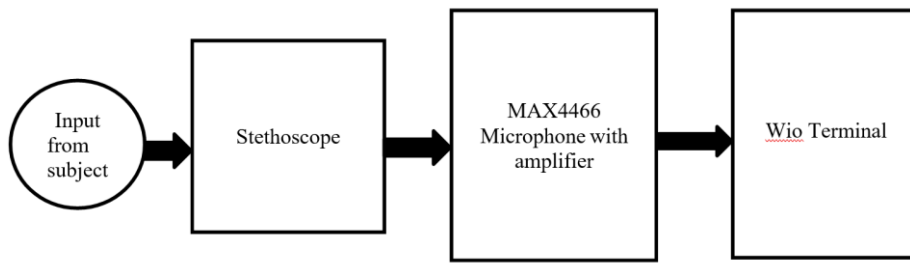
Fig 3. Block representation of the system

The steps in methodology are as follows:

1. **Building the hardware -** All the components are assembled together and are connected as shown in Fig 8.

2. **Collection of data -** To train an edge impulse model, data is gathered from the open source. Data can be gathered from the built-in prototype once the model has been trained and uploaded in the Wio Terminal. The data collected from open source is uploaded in the Edge Impulse as shown in Fig 4.
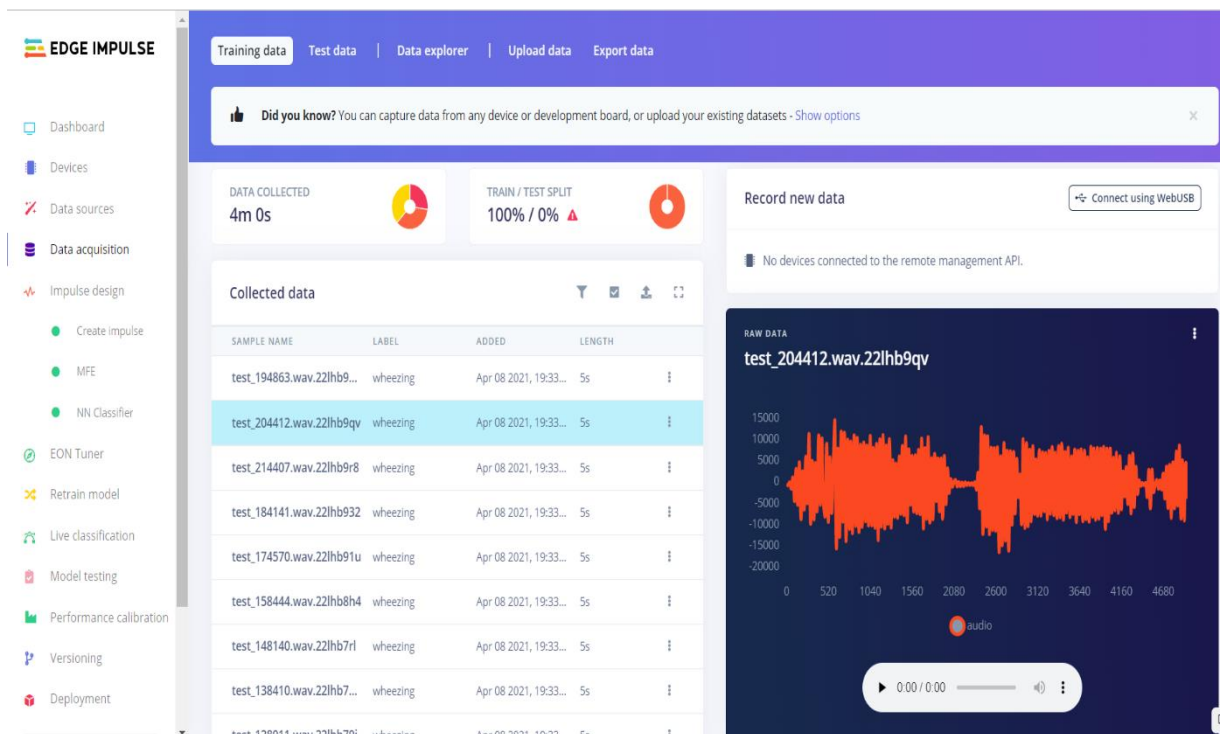

Fig 4. Data uploaded in the Edge Impulse

3. **Building the model -** Edge Impulse is used to create the model. A few parameters, including window size of 1500ms and Frequency of 16000Hz as shown in Fig 5. The model is built utilizing the raw data collected from the open source as shown in Fig 6. The spectrogram as well as confusion matrix are acquired.
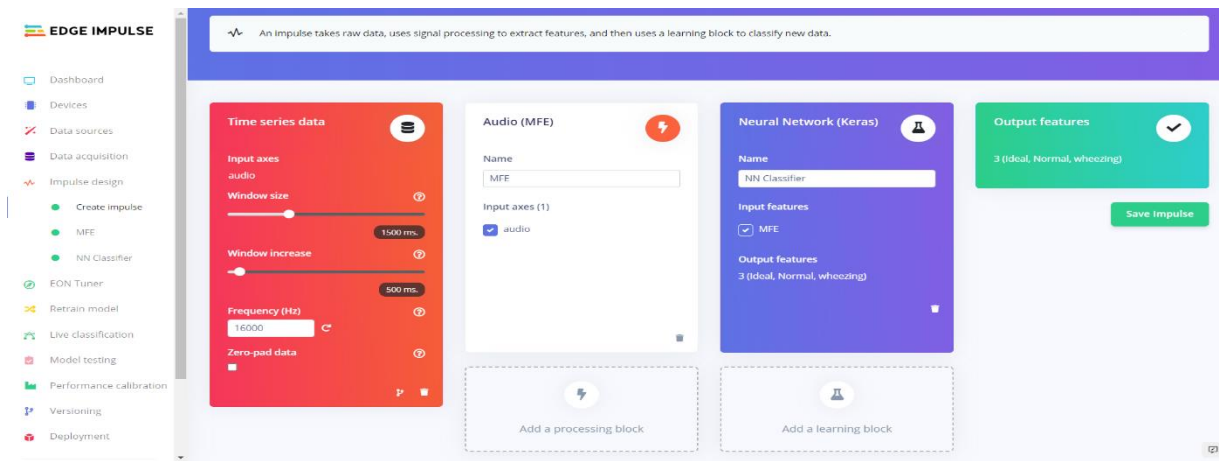
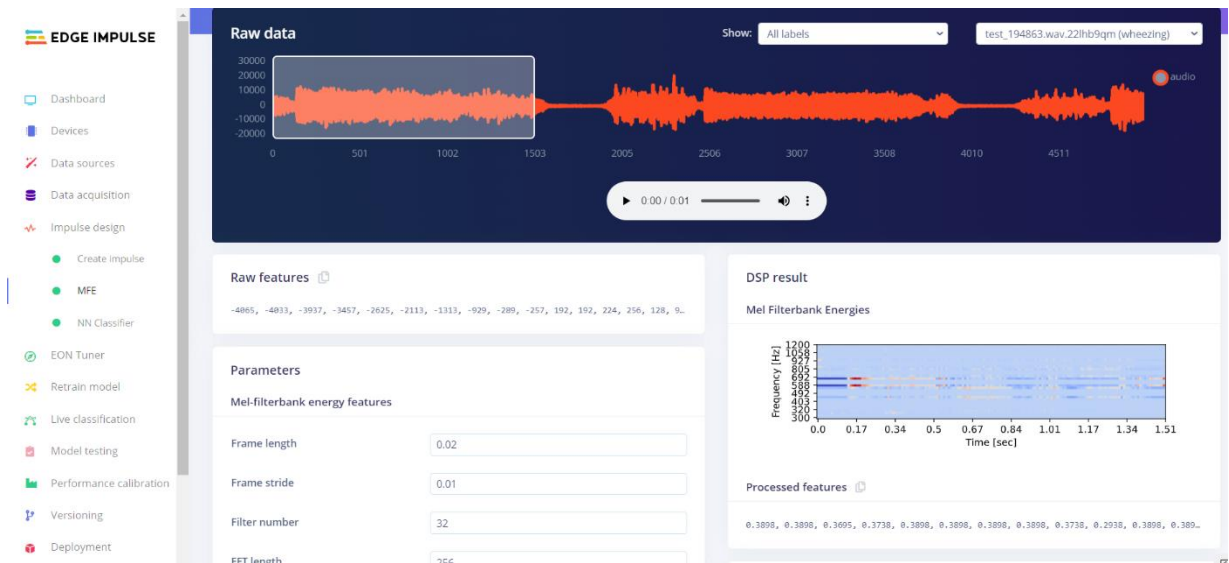Fig 5. Designing an impulse to the model

Fig 6. Building the model

Fig 7.   Accuracy of the developed model

The accuracy of the developed model in edge impulse is tabulated as shown in Fig 7. The developedmodel provides an accuracy of 96.1% among 3 different classes : Ideal, Normal and Wheezing.

4. **Building the firmware -** The firmware is created using the model that was built, the source code,and this is uploaded into the Wio Terminal. The LCD display depicts the classification that is made after analyzing the sound.

This method aids in determining the subject's current status. The components are all interconnected to one another. A stethoscope is used to detect sound, which is then delivered to the MAX4466 amplifier and microphone, which has a high signal-to-noise ratio and adjustable gain. The sound is transmitted to the Wio terminal, which uses the model incorporated into Edge Impulse to classify it. The classification is then displayed on the LCD screen. The collected signal from the microphone is processed in the Wio Terminal according to the edge impulse model. The processed signal is comparedwith the already available signal in the model and based on the comparison the sound is classified. The system's pin diagram is displayed as shown in Fig 8.
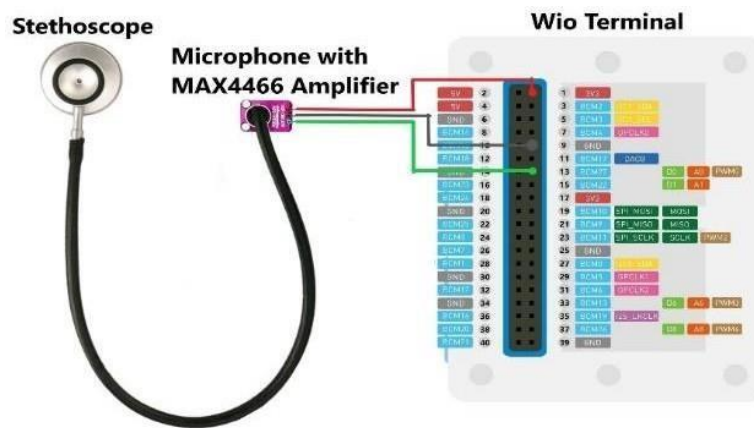

Fig 8. Pin Diagram of the system

(Courtesy: https://www.hackster.io/phatta/smart-stethoscope-powered-by-edge-impulse-a09826#team)

IV.   RESULTS AND DISCUSSION

Here, we mainly focus on three main parameters of lung conditions which are: Ideal (ifnot placed in the required position), Normal and Wheezing.

Case 1: Normal Lung Condition

Fig 9. Output displayed on Wio terminal for a normal lung condition.

In this case, the Wio terminal is connected to MAX4466 which is further connected to the stethoscope, and the power supply is provided to the Wio terminal to turn it on. As the terminal turns on it asks to press button 'A' to start the recording, and as the button 'A' is pressed and stethoscope is placed on the chest of a normal subject this output is displayed on the terminal indicating that the subject's lung sounds are normal.
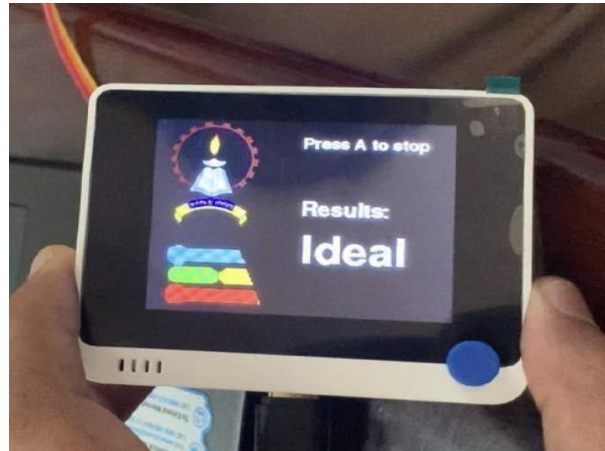
Case 2: Improper placing of stethoscope

Fig 10. Output displayed on Wio terminal for ideal condition

In this case, the Wio terminal is connected to MAX4466 which is further connected to the stethoscope and the power supply is provided to the Wio terminal to turn it on. As the terminal turns on it asks to press button 'A' to start the recording, and as the button 'A' is pressed and stethoscope is not placed on the right position on the chest of a subject this output is displayed on the terminal saying that the stethoscope is not placed in the right position displaying 'ideal'.
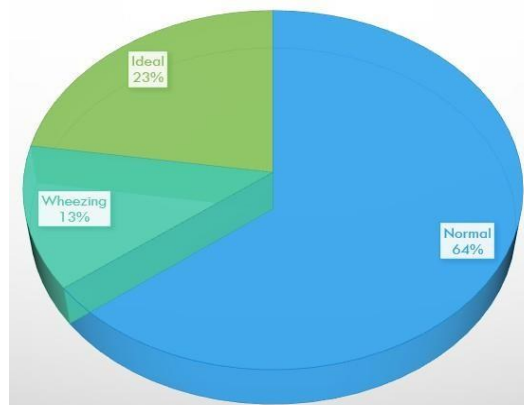

Fig 11. Pie chart representation of subjects with wheezing, ideal and normal

We have taken the sample data of 30 subjects from the prototype and have observed 13% wheezing, 23% ideal and 64% normal sounds from the subjects and the graph is plotted accordingly. Around 19 subjects were classified as normal, 4 subjects as wheezing and 7 subjects were classified as ideal as the stethoscope was not kept at proper position.

V.   CONCLUSION

In the proposed system, a standard stethoscope is combined with a microphone that records the respiratory system's sound and classifies audio at the edge of a microcontroller. To obtain reliable acoustic data, we must make sure that the data being examined is free of any irregularity caused by power line interference, motion artefacts, etc. A filtering system that includes low pass and high pass filters and adjustable gain has been included. The filtered signal is next pre-processed using the Audio MFE processing block, which extracts temporal and frequency characteristics from the signal and feeds them to the neural network. The algorithm then classifies the recording into one of three categories: Ideal (Stethoscope not being used), Normal (No lung abnormalities), and Wheezing. The model is developed and is better than the existing ones as the result is displayed within few seconds, it is built with low cost and minimal components. The connections are simple enough that even non-technical people can construct this model in less time.

REFERENCES

[1] Mehmet nasuhcan et.al "Smart Stethoscope", IEEE Xplore,2021.

[2] Shreyas S. Joshi, Manoj R. Patil, Nikhil P. Kanawade, Aparna P. More, "Bluetooth-based wireless digital stethoscope", International Conference on Emerging Smart Computing and Informatics (ESCI), 2021.

[3] J. Acharya and A. Basu, "Deep Neural Network for Respiratory Sound Classification in Wearable Devices Enabled by Patient Specific Model Tuning", IEEE Transactions on Biomedical Circuits and Systems, vol. 14, no. 3, pp. 535-544, Jun. 2020.

[4] Yu-Jin Lin, Chen-Wei Chuang, Chun-Yueh Yen, Sheng-Hsin Huang, Ju-Yi Chen and Shuenn-Yuh Lee, "An intelligent stethoscope with ECG and heart sound synchronous display", IEEE International Symposium on Circuits and Systems (ISCAS), 2019.

[5] Muhammad E.H. Chowdhury , Amith Khandakar , Khawla Alzoubi ,Samar Mansoor, Anas M. Tahir , Mamun Bin Ibne Reaz and Nasser Al-Emadi "Real-Time Smart-Digital Stethoscope System for Heart Diseases Monitoring",Sensors, MDPI, 2019.

[6] Szot, S., Levin, A., Ragazzi, A. and Ning, T, "A wireless digital stethoscope design", 14th IEEE International Conference on Signal Processing (ICSP), pp. 74-78, 2018.

[7] Gorkem Serbes, Sezer Ulukaya and Yasemin P. Kahya, "An automated lung sound preprocessing and classification system based on spectral analysis methods", Precision Medicine Powered by Health and Connected Health, pp.45-49, January 2018.

[8] K. Kochetov, E. Putin, M. Balashov, A. Filchenkov, and A. Shalyto, "Noise masking recurrentneural network for respiratory sound classification," in International Conference on Artificial Neural Networks. Springer, 2018, pp. 208–217.

[9] Lin Li, Wenhao Xu, Qingyang Hong, Feng Tong and Jinzhun Wu, "Classification between normal and adventitious lung sounds using deep neural network", 10th International Symposium on Chinese Spoken Language Processing (ISCSLP), pp. 1-5, Oct. 2017.

[10] Shuang Leng, Ru San Tan, Kevin Tshun Chuan Chai, Chao Wang, Dhanjoo Ghista and Liang Zhong, "The electronic stethoscope", BioMed Eng OnLine, 14(1):66, July 2015.

[11] S. Nur Hidayah Malek, W. Suhaimizan Wan Zaki, A. Joret, M. Mahadi Abdul Jamil, "Design and development of wireless stethoscope with data logging function", IEEE International Conference on Control System, Computing and Engineering, pp.132-135, Nov 2013.

[12] Todd R. Reed, Nancy E. Reed, Peter Fritzson, "Heart sound analysis for symptom detection and computer-aided diagnosis", Simulation Modelling Practice and Theory 12, pp.129–146, 2004.

[13] Sergio Franco, "Design with operational amplifiers and analog integrated circuits" 3rd edition, mcgraw-hill, ISBN: 0071121730, 9780071121736, 2002.

[14] Leontios J. Hadjileontiadis, Stavros M. Panas, "A wavelet-based reduction of heart sound noise from lung sounds", International Journal of Medical Informatics, vol.52, pp.183–190,1998.

[15] Martin Kompis and Erich Russi, "Adaptive heart-noise reduction of lung sounds recorded by a single microphone", Engineering in Medicine and Biology Society, 1992. Vol.14., Proceedings of the Annual International Conference of the IEEE. Volume: 2, Page(s): 691–692, 1992.

[16] Vijay K. Iyer, P. A. Ramamoorthy, Hong Fan and Yongyudh Ploysongsang, "Reduction of heart sounds from lung sounds by adaptive filtering", IEEE Transactions on Biomedical Engineering, vol. BME-33, no. 12, pp. 1141-48, December 1986.

Machine learning approach for analysis of hematologic diseases in pediatric patients

Shivaprasad Susmita[1]
Student, M-Tech, Medical Informatics,
Dept. of Biomedical Engineering,
Manipal Institute of Technology,
Manipal Academy of Higher Education (MAHE),
Manipal, Karnataka, India

Palkar Anisha[2]
Student, M-Tech, Medical Informatics,
Dept. of Biomedical Engineering,
Manipal Institute of Technology,
Manipal Academy of Higher Education (MAHE),
Manipal, Karnataka, India

Shivaprasad Samhita[2]
Student, M-Tech, Medical Informatics,
Dept. of Biomedical Engineering,
Manipal Institute of Technology,
Manipal Academy of Higher Education (MAHE),
Manipal, Karnataka, India

Dr. Niranjan Sampathila[3*]
Associate Professor - Senior Scale,
Dept. of Biomedical Engineering,
Manipal Institute of Technology,
Manipal Academy of Higher Education (MAHE),
Manipal, Karnataka, India.
* niranjana.s @manipal.edu

Abstract

Blood disorders, also known as haematological disorders, can affect one or more parts of the blood. They can be both cancerous and non-cancerous. Hematologic diseases include blood cell tumours, rare genetic disorders, anaemia, sickle-cell illness, HIV, and side effects from chemotherapy or blood transfusions.

Some of the hematologic disorders that are taken into consideration in the data set are some malignant disorders such as: Myelodysplastic Syndrome (MDS), Acute Myelogenous Leukemia (AML), Chronic Myelogenous Leukemia, Acute Lymphoblastic Leukemia (ALL), and (CML) and some non-malignant disorders such as: Fanconi anemia(FA), With X-linked adrenoleukodystrophy, Severe aplastic anemia. These typical childhood hematologic conditions can lead to chronic medical issues as well as acute illnesses, especially in developing children. The main objectives of care are to anticipate and prevent.

Patients with impaired bone marrow function or immune systems may endure hematopoietic stem cell transplantation (HSCT) and they are infused intravenously to restart the generation of new blood cells. Over the past 50 years, a variety of cancerous and non-cancerous disorders have been treated using this technique.

The patient's own cells (autologous transplant) or cells from another person can be used for HSCT (allogeneic transplant), such as from an identical twin, a sibling, an unknown donor, etc

(syngeneic transplant). Bone marrow, umbilical cord blood, and other tissues are potential cell sources blood plasma, and, in rare circumstances, foetus liver.

In order to improve human life, healthcare professionals are successfully using AI-based algorithms and diverse machine learning algorithms. For the purpose of identifying clinical outcomes and their various forms, the Hematopoietic Cell Transplantation (HCT) data set is examined. Transplanting hematopoietic cells is a highly effective therapeutic method for treating many different disorders. A number of various disorders can be effectively treated by hematopoietic cell transplantation.

The study's primary objective is to examine current machine learning applications and to offer potential directions for future research in the development of various Data Analytics tools.

Keywords: Bone marrow transplantation, Allogenic, Machine Learning, Paediatric, Hematologic Diseases.

I.   INTRODUCTION

In this study, figure 1 represents procedure of allogenic treatment. Transplanting hematopoietic stem cells from an unaltered unfamiliar allogeneic donor is employed. An allogenic transplant uses donor stem cells, which are obtained from another person [1].
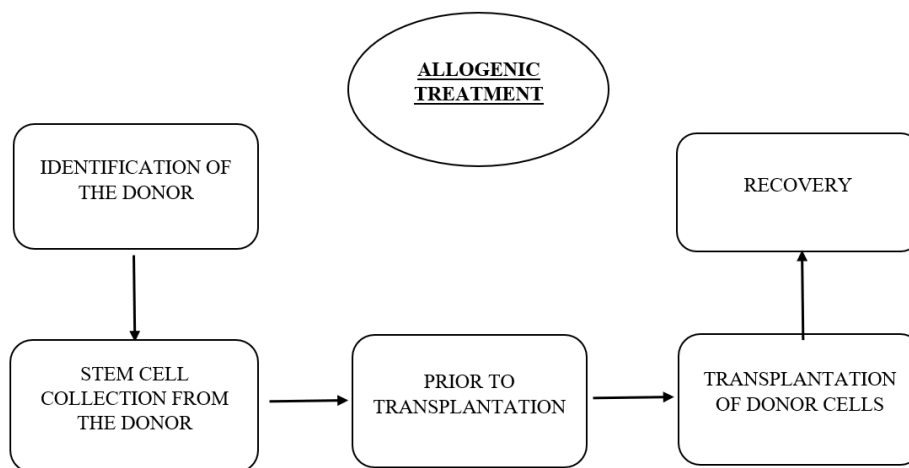

Figure 1: Allogenic treatment procedure [1]

Step 1: Before the process starts, the patients HLA type will be identified through blood testing and the matched must be found. Then, the medical team will next collaborate with the patient to conduct HLA testing on prospective family members who can donate, and if necessary to search through a volunteer database of unconnected donors.

Step 2: The medical personnel will extract cells from the donor's bone marrow or blood. If the cells are taken from the bloodstream, few days prior to the collection of the cells from the blood, to enhance the amount of white blood cells in the donor's blood, daily shots (injections) of medication will be administered. Afterward, from the bloodstream, the stem cells are taken out. If bone marrow is chosen as the source of the cells, the donor will undergo a bone marrow harvest in a hospital.

Step 3: The procedure requires about 5-7 days. To get the patient's body ready to accept the donor cells, they will undergo chemotherapy either with or without radiation therapy.

Step 4: The recipient receives the donor's stem cells after having undergone chemotherapy and radiation treatment or either of them. Through the use of a catheter, the medical personnel administer the donor stem cells to the patient. This is referred to as an ALLO transplant.

Step 5: They are less prone to develop graft-versus-host disease(GVHD) if the donor's proteins closely match their own. The diseased cells are attacked by the transplant's healthy cells.Some of the advantages, disadvantages and common limitations are mentioned in table 1.

Table 1: Advantages, Disadvantages and Limitations of ALLO procedure [2]

Advantages	Disadvantages	Limitations
The host cells will be completely replaced by the donor cells.	Difficulty in finding matched donors	The treatment is expensive.
There might be no requirement of genetic modification.	Requirement of 100% donor chimerism.	When there are resource limited settings it's not feasible.
Possibilities of eliminating viral hosts.	Immunosuppressive treatment and GVHD increase the risk of morbidity/mortality.	It's associated with morbidities/mortalities.

The goal of the dataset was to determine what variables were most crucial in determining whether the transplantation process was successful or not. Testing the assertion that a greater dose of CD34+ cells/kg increases total time of survival without simultaneously producing unfavourable consequences that lower patients' quality of life was the specific goal [1]. There are about 39 attributes used and 187 instances. The data set has some missing values involved.

The main goal of this study is to investigate the various methodology that can be used to analyse the survival rates of paediatric patients with various hematologic diseases subjected to bone marrow transplant.

II.   RELATED WORK AND METHODS USED

Machine learning technology provides methods for processing data in meaningful ways that go beyond what the human brain can comprehend. In the medical literature, more and more terms like deep learning, machine learning, artificial intelligence, and precision medicine are being used [6].

Computer programmes that emulate and imitate human intellect, such as addressing issues and learning, are known as artificial intelligence. The automatic detection of patterns in data is a function of machine learning, an aspect of artificial intelligence. When first introduced, it was described as a software that, rather than having the behaviour explicitly specified, learns to perform a task automatically through experience (i.e., data) [6].

False alarm detection, drug development, entertainment suggestions, pattern recognition, speech-to-text and text-to-speech conversion, entertainment suggestions, forecasting soil moisture, video surveillance, etc. are all applications of machine learning [5].

Some of the advantages, disadvantages and common limitations are mentioned in table 2. Figure 2 represents the flowchart of the general process of machine learning algorithm.

Table 2: Advantages and disadvantages of Machine learning algorithms [5]

| Advantages of ML algorithm	Disadvantages of ML algorithm
Human intervention not needed while writing programme.	Significant number of resources are required to perform algorithms.
Since they are adept at identifying patterns, basic methods are used to anticipate diseases and make suggestions for e-commerce websites.	Its challenging and time-consuming operation since selection of an accurate ML algorithm can be difficult and one must identify the ML method with highest accuracy and apply all of them.
They are able to manage massive, multidimensional "big data."	The biassed training data set used by the ML algorithm may occasionally lead the anticipated result to be inaccurate.
Since algorithms are always improving as a result of the knowledge received through data collection, evaluation criteria like accuracy, specificity and sensitivity, are high.	Critical thinking must be used when creating applications and analysing the results.
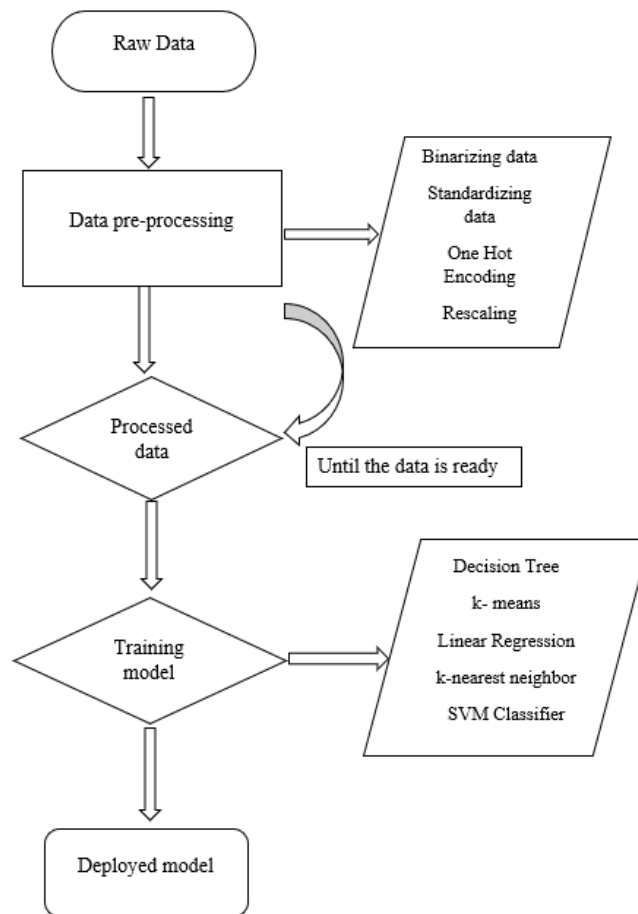
Figure 2: General process of machine learning algorithm [5]

(1) *Survival Prediction of Children Undergoing Hematopoietic Stem Cell Transplantation Using Different Machine Learning Classifiers by Performing Chi-squared Test and Hyper-parameter Optimization: A Retrospective Analysis [3]*

According to the paper writen by Nishat, Mirza Muntasir et al., in addition to predicting bone marrow transplant (BMT) recipients' survival, machine learning (ML) tools have also been shown to be beneficial in identifying the factors that restrict their resilience [3].

This study's goal was to develop an effective classification technique for estimating the survival of children undergoing BMT using a publicly accessible dataset. With an 80-20 split for training and testing, a number of supervised machine learning techniques were examined in this regard. Only the best 11 features out of the 59 features in the dataset were taken into account using the Chi-square feature selection method to assure prediction with the least amount of effort and resources. The grid search cross-validation (GSCV) approach was used in hyper-parameter optimization (HPO) to further increase prediction accuracy. Using a mix of default and optimised hyperparameters, four tests (A, B, C, and D) were run on the original and reduced datasets [3].

Prior to being employed in ML models, the dataset underwent a number of pre-processing processes. The missing values in the dataset were filled in using the average scores for numerical missing values and the most frequent values for categorical missing values. Since ML models are unable to handle categorical data, the categorical variables were converted into a numerical form. The dataset was divided into train and test sets, each of which contained 80:20 of the total data. ML algorithms, including decision tree (DT), logistic regression (LR), random forest (RF), gradient boosting classifier (GBC), k- nearest neighbors (KNN), XGBoost classifier (XGB), and AdaBoost classifier (AdB), were fed into this dataset, where they were trained, and performance metrics were collected [3]. Figure 3 represents the process workflow.
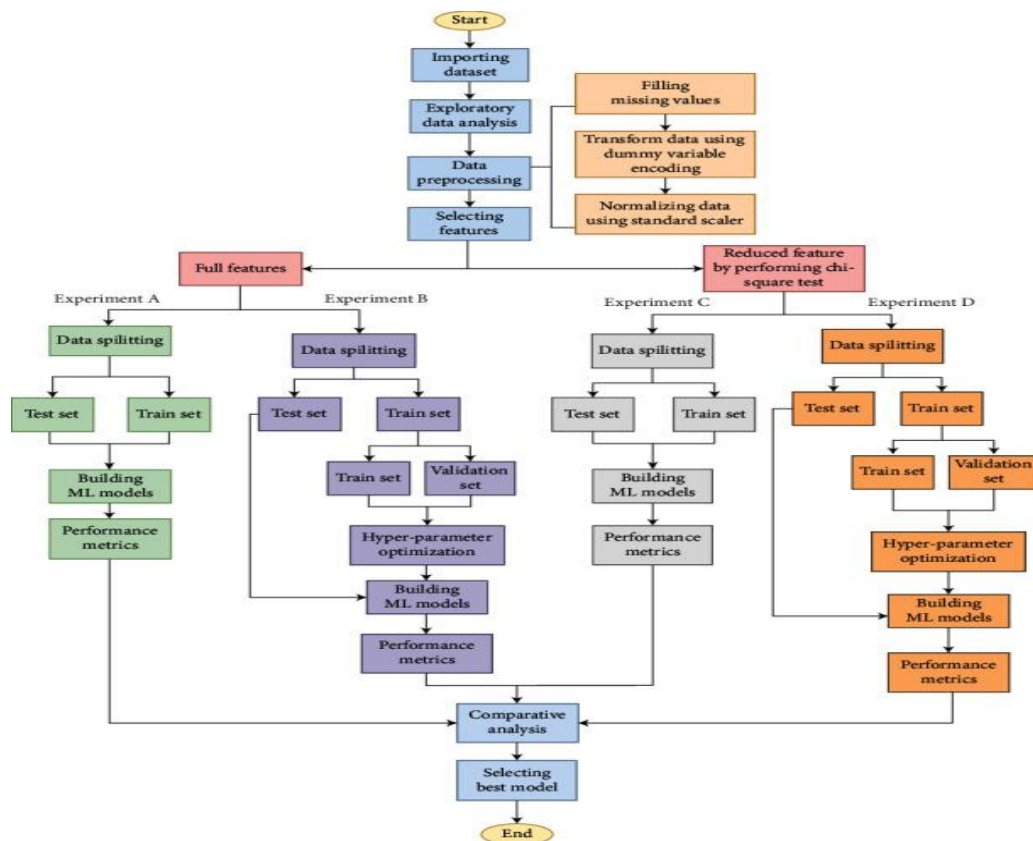

Figure 3: Process flowchart [3]

Very important variables are additionally determined using the Chi-squared statistical test, additionally, the test results are displayed in the supporting materials. A minimum set of traits that can still accurately predict survival is identified after the Chi-squared score has been computed, requiring less computer resources and digitised health data. Thus, the top 11 attributes were randomly chosen from the Supporting Materials and tested for model prediction of association using these 11 features [3].

The following list summarises the study's contributions:

(a) building a suitable statistical model from raw data,

(b) the identification of key factors influencing post-BMT survival,

(c) tackling dimensionality concerns to improve prediction accuracy [3].

(2) Decision rules in survival analysis of patients with hematologic diseases [4]

Significant part of medicine is the analysis of patient survival. In this study, it enabled the authors to evaluate the impact that patient features and chosen treatments have on patient survival. Therefore, an accurate and timely diagnosis as well as an effective treatment plan are crucial. Selected data mining techniques may be useful in this situation to help the doctor. Data from 187 paediatric patients with hematologic disorders were examined in the current study.

 The initial stage of the experiment involved choosing patient features and the most significant impact on survival came from counting techniques. The accuracy of the two models was then compared. The first model had all features, whereas the second used feature selection. Extraction of decision rules was the last phase [4].

The second phase of the research involved creating models that took into account all aspects that were accessible as well as features that were distinguished by the choice of attributes. The categorization was then used to see if the results of the feature selection were as anticipated. Specifically chosen approaches were employed for classification:

- CART (Classification and regression tree).
- C4.5 – a decision tree construction algorithm that is an enhanced iteration of an ID3 algorithm.
- JRip (RIPPER) – is a version of the Repeated Incremental Processing to Obtain Error Reduction procedure.
- PART – an algorithm that builds a partial decision tree as the foundation for knowledge discovery and rule discovery.
- Random Tree – consists of building several Decision Trees from a random collection of datasets [4].

Testing, training, and validation all made use of a 10-fold cross-validation. The individual classifiers were evaluated using Total Accuracy (ACC). Making choice rules was the last phase in the study process. Conclusion IF condition is true. The rule's anticipation or precondition is denoted by the IF part (left side), while the rule's consequence is denoted by the THEN section (right side) [4].

III. RESULTS AND DISCUSSION

From research paper 1:

The total study consisted of four studies using four distinct algorithms. Experiment A without HPO utilised the complete feature dataset as well as the precision, F1 score, recall, AUC ROC were all found to be 94.73%. (0.953) [3].

The best algorithms in terms of accuracy are DT, GBC, LR and AdB. Although the greatest accuracy in trial B was 94.73%, the precision, F1 score, recall, and ROC AUC were all 1, 0.9545, 0.9523, and 0.9467, respectively. The successful methodologies were the similar as in experiment A, however this experiment's overall performance was enhanced because HPO was carried out using the 10-fold GSCV approach [3].

While on the other side, the results of the Chi-square test are used to guide the execution of the experiments C and D. The dataset's top 11 features were taken out, and these experiments used a smaller dataset that only contained those features. KNN showed the highest accuracy in experiment C, with a precision of 0.9047, F1 score of 0.9268, recall of 0.95 and ROC AUC (0.9229) [3].

The similar condensed dataset used in experiment C was used for experiment D's HPO. This time, all ML algorithms performed substantially better than before, with DT having the greatest performance metrics. The accuracy, precision, F1 score, recall and ROC AUC performance metrics for DT in experiment D are as follows: accuracy (0.9473), precision (0.9523), recall (0.9523), and (0.9467) [3].

Based on the results of the aforementioned four tests, It is obvious that HPO is necessary for improving the efficiency of the ML algorithm and that the Chi-square test is a helpful tool for determining the feature that matters the most. The analysis showed that, while requiring little time and effort, top eleven HPO attributes had similar prediction accuracy (94.73%) as the full dataset while using default values [3].

From research paper 2:

For every feature selection approach, the top 16 qualities were chosen. After comparing the resulting qualities, only those that were repeated by each approach were chosen for further investigation. The remaining characteristics were eliminated [4]. Figure 4 represents the Total accuracy (ACC) results comparison for specific models for the attributes mentioned above.

The model with all characteristics and the CART classifier yielded the highest Total Accuracy. The model for algorithm C4.5 with sixteen features produced the same outcome. As can be shown, applying attribute reduction boosted accuracy for algorithms C4.5, Random Tree and PART by many percentage points [4].
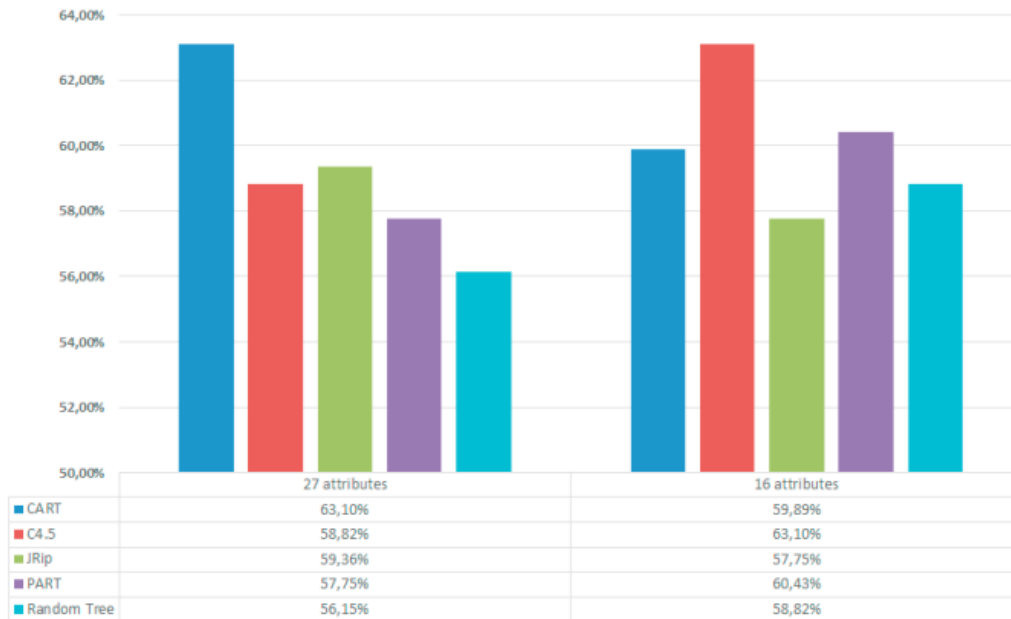
Figure 4: Total Accuracy (ACC) Results Comparison for Individual Models [4]

Decision rules were constructed using the aforementioned methods. Comparisons were made between the rules that were discovered for the models with all argument and those that were discovered for the model after feature reduction. The majority of the time, the rules were the same, which might be a sign of the advantages of attribute selection. Some examples of the chosen decision-making criteria are given as [4]:

☐ IF Relapse = 1 AND RecipientRh = 1 THEN survival status = dead

☐ IF Relapse = 1 AND RecipientRh = 0 AND CMVstatus = 3 THEN survival status = dead

☐ IF Relapse = 0 AND Disease = ALL AND Txpostrelapse = 0 THEN survival status = alive

☐ IF Relapse = 0 AND Disease = ALL AND Txpostrelapse = 1 THEN survival status = dead

☐ IF Relapse = 0 AND Disease = chronic AND RecipientRh = 1 AND HLAgrI = 0 AND ABOmatch = 1 THEN survival status = alive

☐ IF Disease = AML AND CMVstatus = 2 THEN survival status = alive

☐ IF Disease = chronic AND Antigen = 0 THEN survival status = dead

☐ IF Disease = chronic AND HLAmatch = 0 THEN survival status = alive [4]

IV. CONCLUSION

Every year, more transplants are performed; this includes both the donors and the indications. Machine-learning methods will become more necessary to integrate patient data quantities that are too large for humans to handle. Overall, there is reason for optimism, and we anticipate that in the years to come, artificially smart decision assistance tools will be used more frequently in therapeutic settings.

REFERENCES

1. Cancer.net (2019). https://www.cancer.net/navigating-cancer-care/how-cancer-treated/bone-marrowstem-cell-transplantation/what-bone-marrow-transplant-stem-cell-transplant. [Accessed 9 Dec. 2022].

2. Younan, P., Kowalski, J. and Kiem, H.-P. (2013). Genetic Modification of Hematopoietic Stem Cells as a Therapy for HIV/AIDS. Viruses, 5(12), pp.2946–2962. doi:10.3390/v5122946.

3. Ratul, I.J., Wani, U.H., Nishat, M.M., Al-Monsur, A., Ar-Rafi, A.M., Faisal, F. and Kabir, M.R. (2022). Survival Prediction of Children Undergoing Hematopoietic Stem Cell Transplantation Using Different Machine Learning Classifiers by Performing Chi-Square Test and Hyperparameter Optimization: A Retrospective Analysis. Computational and Mathematical Methods in Medicine, 2022, pp.939-1136. doi:10.1155/2022/9391136.

4. Zdrodowska, M. and Dardzińska-Głębocka, A. (2022). Decision rules in survival analysis of patients with hematologic diseases. Procedia Computer Science, 207, pp.3264–3270. doi:10.1016/j.procs.2022.09.384.

5. Molassiotis, A., Van Den Akker, O.B.A. and Boughton, B.J. (1997). Perceived social support, family environment and psychosocial recovery in bone marrow transplant long-term survivors. Social Science & Medicine, 44(3), pp.317–325. doi:10.1016/s0277-9536(96)00101-3.

6. MacEachern, S.J. and Forkert, N.D. (2021). Machine learning for precision medicine. *Genome*, 64(4), pp.416–425. doi:10.1139/gen-2020-0131.

Instruction to Authors

Papers dealing with original research work of basic as well as applied, Biomedical device, Instrumentation, Biomaterial and Tissue engineering, Medical Imaging, Bio mechanic, Rehabilitation, Medical Information, AI and Big Data incorporating new ideas and concepts, novel developments of experimental/ practical significance and theoretical work dealing with aspects of Bio-medical and Life Science Engineering Journal. Review/Tutorial Papers describing the state of art of any particular topic/areas of Bio-medical Engineering are also welcome.

Manuscript Preparation

1. Manuscript should be type written and double spaced single column with adequate margins.
2. The abstract should reflect / highlight the reported work and should not more than 200 words.
3. The Cover page should contain the title, author's name, affiliationand mailing address. A separate list of figure caption should be marked clearly on each illustration.
4. Original Illustration in Indian Ink/Photographs must be sent to the Editor upon receipt of acceptance of the manuscript for publication in the journal.
5. Reference should appear in a separate reference section at the end of the paper with items referred to be numerals in square brackets.References must be complete in all aspects-author's name, title, periodical, volume, inclusive page numbers, month, year etc.

Submission of Manuscript:

1. Authors should submit three copies of the manuscript each complete with abstract, reference and illustration to the Editor of the journal.
2. The Editor upon receipt of manuscript acknowledges the author and will complete the review process. The Editor then communicates to the author, the decision concerning the manuscript.

Biomedical Engineering Society of India

Website: www.Bmesi.org.in

The Biomedical Engineering Society of India is an Organization with members having principal professional interest in Biomedical Engineering. Members from academic institution, R &D organizations, biomedical industry and individuals with sufficient interest in biomedical engineering are eligible for membership in the society upon payment of suitable membership fee (individual life membership Rs. 1520/, Institutional life membership Rs 15200/.